

Stimulated Raman Scattering Microscopy for High-Contrast Drug Imaging

Terumasa Ito

Department of Biomedical Engineering, Tokyo University of Agriculture and Technology, 2-24-16 Naka-cho, Koganei, Tokyo, Japan
Author e-mail address: teru-ito@cc.tuat.ac.jp

Abstract: Real-time, quantitative measurements of a small amount of drug in tissue imaging by conventional Raman microscopy remain challenging. I present a novel stimulated Raman scattering (SRS) microscopy method with increased signal contrast using phase-modulation (PM) and temporal optical filtering. In addition to removing nonlinear background signals with PM, the new microscopy can also reduce intrinsic tissue Raman background signals by temporally separating the excitation and detection processes.

1. Introduction

Noninvasive and label-free laser measurements that acquire information in cells and tissues are applied in many fields of life science and medicine. Raman microscopy, which is based on the frequency characteristics of light scattering mediated by molecular vibration (Raman spectrum), is a promising label-free method for observing pharmacokinetics of small-molecule compounds. However, conventional Raman microscopy does not support real-time analysis due to its weak signals. To address this problem, advanced Raman microscopes utilizing nonlinear effects such as stimulated Raman scattering (SRS), which greatly enhances the Raman signal using pulsed optical excitation, have been developed [1]. While SRS microscopy enables high-speed imaging of living cells and tissue, it is still difficult to quantify a small amount of small-molecule drug. This is because the signal of drug molecules at low concentrations, such as those present in living cells and tissue, is often weak compared to the background signal. Typical background signals that hinder measurement include the non-Raman signals derived from nonlinear effects (such as cross-phase modulation), and the false Raman signals from the living tissue itself. To suppress these unwanted signals, several background suppression methods based on differential spectral detection such as frequency-modulated SRS detection have been proposed [1]. However, quantitative drug measurement remains challenging with the previous methods because differential spectral detection produces large baseline offsets, especially when a steep spectral background overlaps the target signal peak.

We developed a new SRS microscopy method with phase-modulation (PM) and temporal optical filtering [2-3]. In addition to removing the nonlinear background signals using PM detection, the new SRS microscopy can reduce tissue Raman background signals by temporally separating the excitation and detection processes. With this new approach, quantitative drug measurement with a high signal-to-background ratio can be achieved even when the concentrations of the drug molecules are below a few mM in tissue.

2. Results and Discussion

Figure 1 shows a demonstration measurement of drug penetration into skin tissue. To implement the temporal optical filtering, we used a pump-probe scheme with impulsive excitation (pulse width <15 fs) and temporally delayed (delay: 1.7 ps), asymmetrically shaped picosecond pulses, which enables selective detection of the long-lived vibrational signals from the drug molecules. Two topical pain-relief drug solutions (lidocaine hydrochloride: LID, loxoprofen sodium: LOX) were applied to a skin tissue model (Epiderm Epi-606X, Mattek), and the subsequent drug penetration was observed by depth-resolved SRS and confocal reflection imaging. The results showed that the contrast enhancement over conventional SRS was > 40 times, and the limit of detection in tissue was at several mM.

References

- [1] J. X. Cheng, W. Min, Y. Ozeki and D. Polli, Stimulated Raman Scattering Microscopy: Techniques and Applications, Elsevier (2021).
- [2] T. Ito, Y. Obara, and K. Misawa, APL Photon. **3**, 092405 (2018).
- [3] T. Ito, R. Iguchi, F. Matsuoka, Y. Nishi, T. Ogihara, and K. Misawa, Biomed. Opt. Express **12**, 6545-6557 (2021).

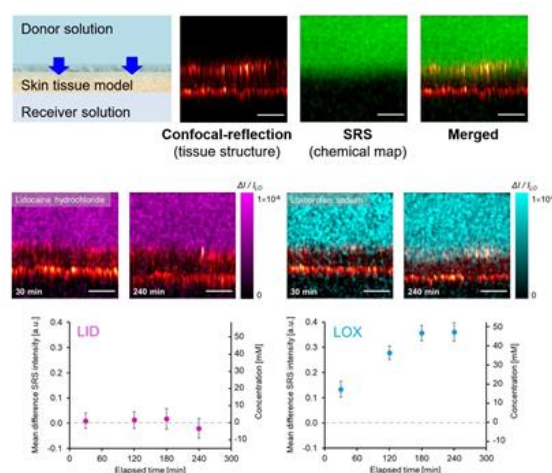


Fig. 1 SRS imaging of drug penetration into skin tissue: (top) depth-resolved imaging using combined confocal reflection and SRS, (middle) 30 and 240 minutes after topical application of 148 mM LID, and 131 mM LOX (LID at 1092 cm^{-1} , LOX at 1184 cm^{-1} , scale bar: 50 μm), (bottom) monitoring of drug concentrations in tissue, showing that the LOX was more permeable to the skin.

Few cycle THz dual-pulse generation and manipulation technique with a high degree of freedom

Hao-Keng Wei^{1†}, Zai-Wen Chen¹, Yu-Ting Lin¹, Hironori Ito², Kazuhiko Misawa^{3,4}, Chih-Wei Luo¹

¹Department of Electrophysics, National Yang Ming Chiao Tung University, Hsinchu, 30010, Taiwan.

²Graduate Faculty of Interdisciplinary, Research Faculty of Engineering, University of Yamanashi, Japan.

³Department of Applied Physics, Tokyo University of Agriculture and Technology, 2-24-16 Naka-cho, Koganei, Tokyo, Japan

⁴Department of Biomedical Engineering, Tokyo University of Agriculture and Technology, 2-24-16 Naka-cho, Koganei, Tokyo, Japan

Author e-mail address [†]: ihatetomato.sc05@gmail.com

Abstract: In this study, we demonstrated the THz dual-pulse generation via a modified Michelson interferometer (MI). Comparing to the traditional methods of field control technique, the architecture we proposed here has many advantages such as higher damage threshold, higher tunability, the ability to scale to multi-pulses, etc. Furthermore, we proposed the f - t modulation technique to manipulate the THz dual-pulse via only two parameters. Such novel system shows huge potential for applications, not only in imaging and spectroscopy but also in next-generation communications.

1. Introduction

Field control techniques play a pivot role in many fields such as spectroscopy, imaging, and communications. Our previous work [1] proposed the modified MI system to generate the polarization twisting pulse/dual-pulse (PTP/PTDP) as the light source, which gave high degrees of freedom such that one can arbitrary manipulate the twisting frequency, helicity, and interval between dual-/multi- pulse. Based on this technique, we utilized such PTPs/PTDPs as light source to generate the THz pulses by utilizing an EO crystal (e.g., the GaP crystal in this study) to perform a second-order nonlinear process [2,3].

2. THz generation via PTPs/PTDPs formulism

To characterize the PTPs/PTDPs, the zero-phase diagram is introduced, which indicated the relation between frequency and time delay of a pulse. Such conceptual diagram helps us to realize the key characteristics of a PTP/PTDP such as the rotation frequency and helicity, and straightforwardly links the key parameters of system and pulses such as the first-/second- order dispersion and the position of optical elements.

A PTP can be model by the combination of a right-handed circularly polarized (RHCP) pulse and a left-handed circularly polarized (LHCP) pulse as:

$$\begin{cases} E_x(t) \\ E_y(t) \end{cases} = \int \frac{d\omega}{2\pi} e^{-i\omega t} E_i(\omega) e^{-i\theta_c} \begin{bmatrix} 1 \\ i \end{bmatrix} + \int \frac{d\omega}{2\pi} e^{-i\omega t} E_i(\omega) e^{-i\theta_c} e^{-i\theta_p} \begin{bmatrix} 1 \\ -i \end{bmatrix}, \quad (1)$$

where $E_i(\omega)$ is the spectrum of the initial laser pulse. θ_p and θ_c are the chirp introduced by first- and second- order dispersion (γ, β) from the system, formulated by $\theta_p = \gamma(\omega - \omega_0)$ and $\theta_c = \beta \frac{(\omega - \omega_0)^2}{2}$.

By calculating the second-order susceptibility of a GaP crystal, the polarization $P = [P_x \ P_y]^T$ induced by a PTP normally incident onto (1 1 1) plane can be shown as [4]:

$$\begin{bmatrix} P_x \\ P_y \end{bmatrix} = \frac{4}{\sqrt{6}} \epsilon_0 d_{14} \begin{bmatrix} -E_x E_y^* - E_x^* E_y \\ E_y E_y^* - E_x E_x^* \end{bmatrix}, \quad (2)$$

where ϵ_0 is the vacuum permittivity, and d_{14} EO coefficient of GaP crystal. E_x, E_y are from equation (1), and E^* represented the complex conjugate of E .

3. Conclusions

In this study we demonstrate the THz generation from PTPs/PTDPs with a high degree of freedom numerically and experimentally. A conceptual zero-phase diagram is introduced to characterize the PTPs/PTDPs, which can be helpful and straightforward to manipulate the PTPs/PTDPs and corresponding THz (dual-)pulse. Such light source shows a huge potential in imaging, spectroscopy, and next-generation communications.

4. References

- [1] H.-K. Wei *et al.* "Generation and manipulation of polarization-twisting dual pulses with a high degree of freedom," *Opt. Lett.* **45**, 6663-6666 (2020)
- [2] H.-K. Wei *et al.* "Few-cycle THz wave manipulation with a high degree of freedom via f - t modulation," *Opt. Lett.* **48**, 1016-1019 (2023)
- [3] Q. Chen *et al.* "Electro-optic transceivers for terahertz-wave applications," *J. Opt. Soc. Am. B* **18**, 823-831 (2001).
- [4] M. Sato *et al.* "Terahertz polarization pulse shaping with arbitrary field control," *Nat. Photonics* **7**, 724-731 (2013).

Energy transfer between Alq₃ molecules and Si revealed by pump-probe spectroscopy

Yu-Chan Tai¹, Wen-Yen Tzeng^{1,2}, Jhen-Dong Lin¹, Fu-Xiang Chen¹, Yi-Hou Kuo¹, Ruei-Jhe Tu¹,
Ming-Yang Huang¹, Shyh-Shii Pai³, Nick Weihan Chang³, Sheng-Yang Tseng³,
Chi Chen⁴, Chun-Liang Lin¹, Shun-Jen Cheng¹, Chih-Wei Luo^{1,5,6,7,8}

¹Department of Electrophysics, National Yang Ming Chiao Tung University, Hsinchu 300, Taiwan.

²Department of Electronic Engineering, National Formosa University, Yunlin 632, Taiwan.

³FAB 12B, Taiwan Semiconductor Manufacturing Company, Ltd., Hsinchu 300, Taiwan.

⁴Research Center for Applied Sciences, Academia Sinica, Taipei, 115, Taiwan.

⁵Institute of Physics and Center for Emergent Functional Matter Science, National Yang Ming Chiao Tung University, Hsinchu 300, Taiwan.

⁶National Synchrotron Radiation Research Center, Hsinchu 300, Taiwan.

⁷Taiwan Consortium of Emergent Crystalline Materials (TCECM), National Science and Technology Council, Taiwan.

⁸Department of Physics, University of Washington, Seattle, Washington 98195, USA.

brianyjtai1994.sc08@nycu.edu.tw; cwluoep@nycu.edu.tw

Abstract: We utilize ultrafast optical pump-probe spectroscopy to uncover energy transfer mechanisms between Alq₃ organic molecules and Si semiconductors. The 400-nm pump and 800-nm probe spectra provide comprehensive insights into SiO₂-thickness-dependent carrier relaxation across Si's continuous band, while the 400-nm pump with broadband-probe spectra depict carrier population relaxation at multiple energy positions in Si's conduction band. The presence of Alq₃ distinctly influences Si recombination dynamics, underscoring their interplay. We ascribe Si's carrier dynamics alterations to nonradiative energy transfer, comparing the mechanisms to theoretical dipole-dipole interactions.

OCIS codes: (320.7130) Ultrafast processes in condensed matter, including semiconductors; (320.7150) Ultrafast spectroscopy.

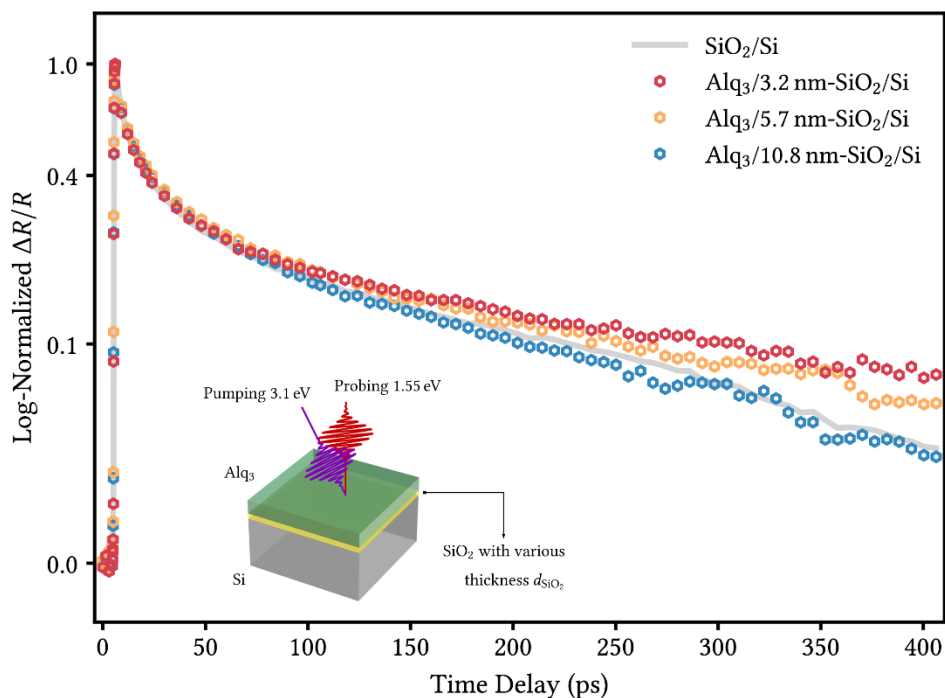


Figure 1: The presence of an Alq₃ thin film significantly influences the photoexcited ultrafast carrier dynamics of Si compared to the intrinsic Si carrier dynamics represented by the solid line. Scatter plots in three sets illustrate how Si's carrier dynamics are modulated based on SiO₂ thickness. The inset image depicts the schematic structure of the Alq₃/SiO₂/Si sample.

Ultrafast Time-resolved and Vibrational Dynamics of Native and nitrosylated (NO-) Cytochrome *c*

Ying Kuan Ko¹, Atsushi Yabushita^{1,2} and Takayoshi Kobayashi^{1,2,3,4}

¹Department of Electrophysics, National YangMing ChiaoTung University, Hsinchu, Taiwan

²Research Institute for Engineering, Kanagawa University, Kanagawa, Japan

³Brain Science Inspired Life Support Research Center, The University of Electro-Communications, Tokyo, Japan

⁴Research Center for Water Frontier Science and Technology, Tokyo University of Science, Tokyo, Japan
kentko78@gmail.com

Abstract: Using a homemade sub-10 fs broadband NUV laser pulses system, the primary reaction mechanism of native and nitrosylated cytochrome *c* (Cyt *c*) were elucidated for two redox forms of ferric (oxidized) and ferrous (reduced) Cyt *c* by measuring their transient absorption (TA) spectra. The TA traces measured in the broad probe wavelength region were analyzed by the global analysis method to study the electronic dynamics. With the temporal resolution of 10 fs, we observed TA signal modulation caused by the molecular vibration in the time domain, which can be used to calculate the instantaneous frequency of the molecular vibration mode.

Introduction

Cytochrome *c* (Cyt *c*) is a widespread hemeprotein in mammals, which usually are found in inner mitochondrial membrane of cells, which involves in a variety of important biological processes, such as a trigger of apoptosis, an energy transfer of electron transport chain (ETC) and an antioxidant for the cell. The interaction with cardiolipin maintains the normal operation of mitochondria. Cyt *c* is mainly composed of a porphyrin macrocycle and a central ion in redox (ferric, Fe³⁺-Met80) and reduced (ferrous, Fe²⁺-Met80) form. Both two redox forms can transfer to each other while involving the ET reactions. In apoptosis process of cells, nitrosylated (nitric oxide bind-) Cyt *c* plays an important role as a trigger regulates the release of Cyt *c* from mitochondria or increase of its peroxidase activity. These phenomena are associated with the conformational change of heme, the center structure of Cyt *c* [1].

We used time-resolved spectroscopy to investigate the reaction dynamics and processes of native and nitrosylated Cyt *c* in two redox forms [1]. The results reveal that photo-dissociation and recombination between central ion and connected ligand, Fe²⁺-Met80 in ferrous Cyt *c* dominated the ultrafast dynamic after ultrafast pulse excitation (see Fig.1(a) and (c)). On the contrary, the dissociation did not occur in ferric form. In nitrosylated form, photo-dissociation occurred both in two redox forms and the recombination of NO is more slowly compared with native ferrous Cyt *c*. Furthermore, the results of the real-time analysis of vibrational dynamics reveal a swifter tendency for structural recovery following NO dissociation in as compared to Met80. In conclusion, the binding and dissociation of NO dominates the heme conformational changes and ultrafast dynamics of NO-Cyt *c* complex (see Fig.1(b) and (d))

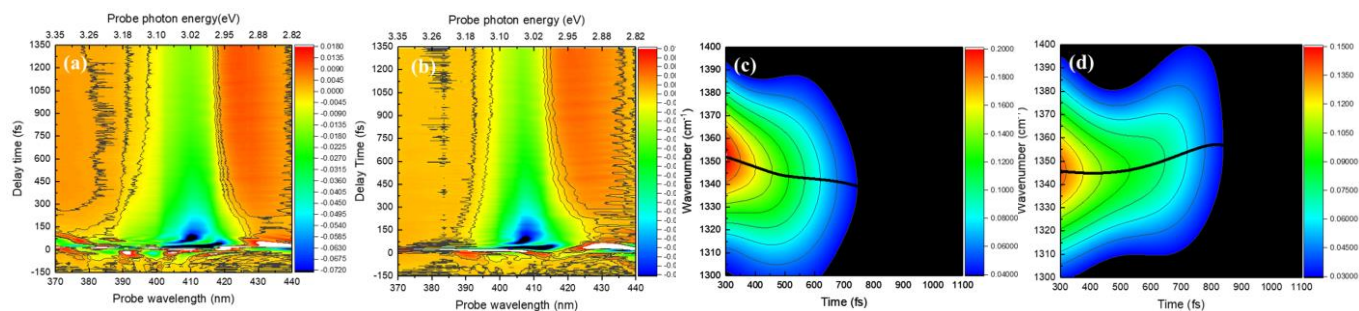


Fig. 1 The transient absorption (TA) spectrum of (a) native and (b) nitrosylated ferrous Cyt *c*, with the corresponding spectrogram traces in (c) and (d) are calculated within the probe wavelength range of 430-440 nm, respectively.

References

[1] Y.K Ko, "Primary Electronic and Vibrational Dynamics of Cytochrome *c* Observed by Sub-10 fs NUV Laser Pulses," J. Phys. Chem. B **124**, 8249–8258 (2020)

The polarization control of coherent mid-infrared pulses generated through the four-wave-mixing filamentation

Wei-Hong Huang^{1*}, Yi-Ruei Sie¹, Chih-Wei Luo¹

¹ Department of Electrophysics, National Yang Ming Chiao Tung University, Hsinchu 30010, Taiwan.

* Author e-mail address: nc7410@gmail.com

Abstract: We demonstrated the polarization control of coherent mid-infrared (MIR) pulses which were generated through the laser-induced two-color filamentation. By manipulating the polarization of injected two-color pulses, the combined two-color laser fields will drive ionized plasma to change the resultant polarization of MIR pulses.

1. Introduction

The optical mid-infrared (MIR) regions have various crucial molecular vibrational mode, which can help researchers to identify the chemical bonds and formations of molecules or crystals. Based on these topics, many research groups are interesting to developing a coherent MIR light sources which had enormous potential to temporally resolve the dynamics of energy transfer between chemical bonds. There is a popular method to generate coherent MIR pulses is to use nonlinear four-wave-mixing (FWM) processes through ionized filamentation which was induced by the two-color laser fields [1,2]. Through the laser-induced air plasma filament, we can have much more smooth dispersion curve in MIR region. Because of that, relatively easier phase matching condition can make ultra-broadband MIR available. In the same time, the low dispersive air plasma and self-compression effect can keep the output MIR pulse well in Fourier transform limit, so the end-user does not need to fix the chirp effect of pulse before the applications.

Straightforwardly, we can easily control the polarization of injected pulses and the resultant laser-induced filamentation will be modified as the field of laser pulses. This experimental control is a common method and widely used in two-color systems, especially for THz generation [3]. In addition, some groups had noted that the generated THz through two-color laser-induced filamentation has abnormal enhancement when the injected two-color pulses were circularly polarized rather than linearly polarized [4,5].

2. Results and discussions

In our work, we had found similar behaviors when the MIR pulses generated by switching to circularly polarized two-color filamentation. As the Fig. 1 shown, different types of dual waveplates (DWP) were employed in our setup to separately control the polarization types of two-color pulses. Fig 1(c,d) showed that the circularly polarized MIR pulses can be generated by DWP_b, a QWPs at 800 nm, but a FWP at 400 nm. The output power of MIR pulse was also enhanced, comparing with the typical waveplates, DWP_a. In summary, according to manipulating the polarization of injected two-color pulses, the combined two-color fields of plasma will drive ionized plasma to different direction, and the resultant dynamic of ions will create four-wave-mixing MIR pulses along with the corresponding direction.

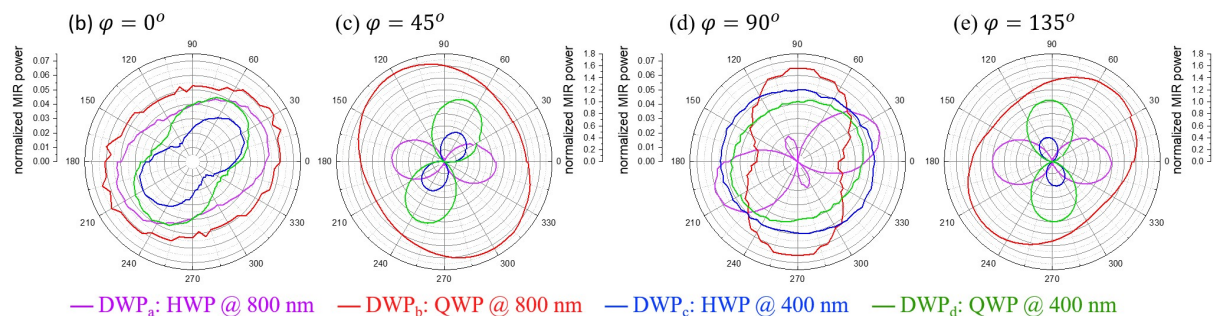


Fig. 1. The power of FWM MIR pulses after passing through a MIR polarizer. The angles of polar coordinates were corresponded to the angle between MIR polarizer and input fundamental pulses. The distances of polar coordinate were with respect to the normalized power of MIR pulses. φ was the angle between DWP and input fundamental pulses.

References

- [1] W.-H. Huang, Y. Zhao, S. Kusama, *et al*, Opt. Express **28**, 36527 (2020).
- [2] Y. Zhao, S. Kusama, Y. Furutani, *et al*, Nat. Commun. **13**, 1077 (2022).
- [3] Z. Zhang, Y. Chen, S. Cui, *et al*, Nat. Photonics **12**, 554 (2018).
- [4] Y.-Y. Tu, C. Meng, X. Sun, *et al*, J. Opt. Soc. Am. B **39**, A83 (2022).
- [5] Q. Song, X. Yuan, S. Hu, J. Huang *et al*, Opt. Express **29**, 22659 (2021).

Hyperspectral imaging using sub-cycle mid-infrared pulses generated through two-color filamentation

Takao Fuji

Laser Science Laboratory, Toyota Technological Institute, Nagoya 468-8511, Japan
fuji@toyota-ti.ac.jp

Abstract: We have demonstrated hyperspectral imaging using sub-cycle mid-infrared pulses generated through two-color filamentation. Up-conversion of the MIR pulse transmitted through the sample at the image plane significantly improve the performance of the spectral imaging.

Hyperspectral imaging integrates imaging and spectroscopy to characterize chemical distributions. The resulting spectral image, a “data cube,” combines two spatial dimensions with one spectral dimension, offering full-spectrum insights from each pixel. The power of mid-infrared (MIR) hyperspectral technique lies in its ability to perform “chemical imaging” or “chemical mapping,” capturing the molecular composition of objects through molecular vibration. However, the efficacy of the MIR hyperspectral imaging is hampered by limited pixels and the low signal-to-noise ratio of MIR detectors.

To overcome these challenges, the concept of up-conversion emerges as a promising strategy. By converting MIR ultrashort pulses into visible or near-infrared light, detection using Si-based detectors becomes feasible, greatly enhancing performance. Prior approaches focused the MIR beam into a nonlinear crystal to generate intense visible light through wavelength conversion at the Fourier plane [1]. However, this method necessitates wavelength-dependent image calibration based on phase matching conditions, hindering efficiency.

In this invited talk, a novel MIR hyperspectral imaging technique based on sub-cycle MIR pulses [2] is introduced. With broad bandwidth spanning functional group ($1500\text{--}3000\text{ cm}^{-1}$) and fingerprint ($500\text{--}1500\text{ cm}^{-1}$) regions, and intense intensity facilitating wavelength conversion at the image plane, this configuration eliminates wavelength dependency in image size. Figure 1(a) illustrates the two imaging types with up-conversion.

Generating sub-cycle MIR pulses (13.4 fs) utilizes four-wave mixing through two-color filamentation [3]. A $\sim 4.4\text{ }\mu\text{m}$ thick GaSe crystal positioned on the sample’s image plane interacts with the MIR pulse passing through the sample and a chirped 800 nm pulse (1.8 ps). This interaction generates a sum frequency signal subsequently captured by a silicon-based hyperspectral camera, producing hyperspectral images for analysis.

Our analytical prowess is validated through imaging and mapping of *A. cepa* bulb leaf epidermal cells. Cells affixed to $200\text{ }\mu\text{m}$ CaF_2 substrates reveal intricate structures illuminated by visible light (Fig. 1(b)), while hyperspectral imaging (Fig. 1(c)) maps cell wall (red), cytoplasm (cyan), and nuclei (green) through MIR spectral analysis. Significantly, nuclei distribution is exclusively visible in the MIR hyperspectral image, underscoring the method’s potential for precise cell analysis. This innovative approach broadens horizons for advanced hyperspectral imaging, particularly in the realm of cellular exploration and characterization.

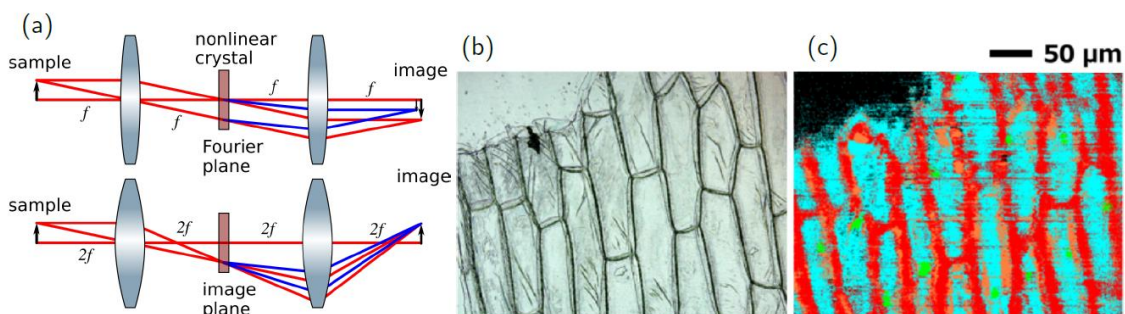


Fig. 1(a) Schematic of the two types of the imaging with upconversion. (b) Microscopy image illuminated by visible light. (c) Mapped hyperspectral images of the onion (*A. cepa*) bulb leaves epidermal cells.

[1] S. Junaid, S. Chaitanya Kumar, M. Mathez, M. Hermes, N. Stone, N. Shepherd, M. Ebrahim-Zadeh, P. Tidemand-Lichtenberg, and C. Pedersen, “Video-rate, mid-infrared hyperspectral upconversion imaging,” *Optica* **6**, 702–708 (2019).

[2] Y. Zhao, S. Kusama, Y. Furutani, W.-H. Huang, C.-W. Luo, and T. Fuji, “High-speed scanless entire bandwidth mid-infrared chemical imaging,” *Nat. Commun.* **14** 3929 (2023).

[3] W.-H. Huang, Y. Zhao, S. Kusama, F. Kumaki, C.-W. Luo, and T. Fuji, “Generation of sub-half-cycle $10\text{ }\mu\text{m}$ pulses through filamentation at kilohertz repetition rates,” *Opt. Express* **28**, 36527–36543 (2020).

Label-Free Imaging of Melanoma with Confocal Photothermal Microscopy

Takayoshi Kobayashi

Advanced Ultrafast Laser Research Center and Brain Science Inspired Life Support Research Center, University of Electro-Communications, 1-5-1 Chofugaoka, Chofu, Tokyo 182-8585, Japan

Abstract: Label-free confocal photothermal (CPT) microscopy was utilized for the first time to investigate malignancy in mouse skin cells. Laser diodes (LDs) with 405 nm or 488 nm wavelengths were used as pumps, and a 638 nm LD was used as a probe for the CPT microscope. A Grey Level Cooccurrence Matrix (GLCM) for texture analysis was applied to the CPT images. Nine GLCM parameters were calculated with definite definitions for the intracellular super-resolved CPT images, and the parameters.

1. Introduction

Malignant melanoma (MM) is one of the most common cancers worldwide. It has a favorable prognosis only if the affected area is removed at an early stage. MM reportedly causes the large majority of skin cancer deaths despite the fact that it accounts for <2% of skin cancer cases [1]. The incidence of MM has been increasing for >30 years and one of its most ominous characteristics is its high propensity to produce distant metastases, because it can get disseminated throughout the body through lymphatic and hematogenous spread. For this reason, early detection and treatment of MM are crucial life-saving measures [2]. Although dermoscopy is a powerful diagnostic technique [3] and the ABCDE (abbreviation for asymmetrical shape, border, color, diameter, and evolution) rule provides a guide to the identification of involved areas, pathological examination is the gold standard for MM diagnosis. But diagnosis remains highly reliant on the skill level of the pathologist.

2. Results

We developed a photothermal microscope with resolution beyond diffraction limit. The textural structure of the images of the mouse skin samples containing both nevus and MM cells taken with the PT imaging method were analyzed by GLCM. The nine parameters were calculated as shown below. The areas of imaging data were analyzed by the GLCM method, and the 8-bit level gray level intensity distribution of the PT signal was obtained. Twelve images of $72 \times 72 \mu\text{m}^2$ to multiple samples of excitation at 488 nm for both nevus and MM samples were also obtained. The areas of imaging data were analyzed by this method, and the 8-bit level gray level intensity distribution of the PT signal was analyzed using the GLCM analysis. There were total of 48 images with an area of $18 \times 18 \mu\text{m}^2$ from both nevus and MM providing sufficient data of various parts of skin. We found that a few of the nine GLCM parameters clearly showed the ability to discriminate between nevus and MM, and can hopefully be used as criteria for pathological diagnosis [4,5].

We then performed receiver operating characteristic (ROC) curve analysis based on fitted Gaussian curves to the observed distribution. An ROC curve is commonly used to evaluate the diagnostic ability of a test. When a threshold parameter used in the system classifying examinees into two groups, positive and negative for some features, this curve is plotted as the sensitivity against the false positive ratio. The d parameter $d = 10$ provides the best performance for all nine GLCM parameters in both cases pumped at 405 nm and pumped at 488 nm. We plotted ROC curves for nine parameters based on the Gaussian curves. The area under the curve (AUC) is an indicator of the diagnostic ability; >0.9 , $0.7\sim 0.9$, and <0.7 correspond to high accuracy, moderate accuracy and poor accuracy, respectively. Entropy, Contrast and Variance show high AUCs, namely 0.909, 0.905 and 0.897, respectively. These values indicate that those parameters provide highly accurate methods to distinguish nevus and MM cells. In the case of 488 nm excitation, the AUCs of Prominence, Variance and Shade are 0.812, 0.808 and 0.768, respectively, indicating not as good performance as 405 nm excitation [4,5].

3. References

- [1] American Cancer Society. Melanoma Skin Cancer Overview. 2015. Available online: <https://www.cancer.org/cancer/melanoma-skin-cancer.html> (accessed on 14 August 2018).
- [2] Rigel, D.S.; Carucci, J.A. Malignant melanoma: Prevention, early detection, and treatment in the 21st century. *CA Cancer J. Clin.* **2000**, *50*, 215–36.
- [3] Soyer, H.P.; Smolle, J.; Kerl, H.; Stetner, H. Early diagnosis of malignant melanoma by surface microscopy. *Lancet* **1987**, *2*, 803.
- [4] Kobayashi T. et al. Resolution enhancement of pump-probe microscope with an inverse-annular filter, *Photonics* (MDPI) **2018**, *25*, 271.
- [5] Kobayashi T. Label-free three-dimensional imaging of melanoma with confocal microscopy: Differentiation between malignant and benign tissue, *Bioengineering*. (MDPI), **2018**, *5*, 67.

Quantum Enhancement for strength of vibrational coupling between an optical cavity and molecules

Fumiaki Matsuoka

Tokyo University of Agriculture and Technology, 2-24-16 Naka-cho, Koganei, Tokyo 184-8588, Japan
fu-matsuoka@go.tuat.ac.jp

Abstract: It has been shown that when the optical modes of the optical cavity and the vibrational modes of the molecules are strongly coupled, the chemical properties of the molecules is changed. Since the strength of vibrational coupling in molecular-cavity systems is mainly determined by the number of molecules, it is difficult to reach the vibrational strong coupling regime for solutes in the liquid phase with low concentration and for the gas phase. In this presentation, we theoretically show that quantum vacuum squeezing has the potential to reduce the number of molecules required for strong coupling conditions by about 1/2 to 1/10 under the realistic or the feasible squeezing condition.

When the energies of the optical cavity modes and the vibrational mode of the molecules are matched in the optical cavity, these modes are coupled even if there are no external electromagnetic fields. In particular, the strength of such vibrational coupling is enough strong for the decay rate of the excited state of the molecules and the decay rate of the cavity, a coupling state called vibrational strong coupling (VSC) is formed [1-8]. Under the VSC formation, molecules in behave differently than those in free space such as accelerating or decelerating organic chemical reactions [2, 3], and modifications of self-assembly [4], etc.

The realization of VSC for various molecules would be important to understand the fundamentals of phenomena and to open new applications. However, since the strength of vibrational coupling in molecular-cavity systems is mainly determined by the number of molecules (i.e. concentration), it is difficult to reach the VSC regime for solutes in the liquid phase with low concentration and for the gas phase.

Here, we consider another approach to enhance the strength of the vibrational coupling. It has been theoretically shown that squeezing of quantum vacuum fluctuations in the cavity field can enhance the coupling strength between the optical cavity field and the two-level system in the cavity [9-11], and such enhancement effect has been experimentally demonstrated in a two trapped ion qubits system to realize quantum gates [12]. While only a two-level system is considered in these demonstrations, it remains unclear whether such a squeezing effect works in many-molecules-cavity coupling system.

In this presentation, we theoretically demonstrate that the number of molecules required for strong coupling conditions can be reduced by quantum squeezing effect of the cavity vacuum field using the Hamiltonian of a many-molecules-cavity coupling system with rotating wave approximation known as the Tavis-Cummings model [5-8]. By applying squeezing operation to this model, we obtain an effective coupling constant $g_{\text{eff}} = (g N^{1/2} e^r) / 2$ where g is the coupling constant, N is the number of molecules and r is the amplitude of the squeezing. In addition, we calculate that the quantum vacuum squeezing has the potential to reduce the number of molecules required for strong coupling conditions [5] by about 1/2 to 1/10 under the realistic or the feasible squeezing condition [13] and using typical parameters [1, 5, 12].

- [1] A. Shalabney, *et al.*, Nature Commun., **6**, 5981 (2015).
- [2] K. Hirai and H. Uji-i, Chem. Lett. **50**, 727-732 (2021).
- [3] F. J. G.-Vidal, *et al.*, Science **373**, 178 (2021).
- [4] K. Hirai, *et al.*, Chem. Sci. **12**, 11986–11994 (2021).
- [5] M. S. Rider and W. L. Barnes, Contemp. Phys. **62** (4), 217-232 (2021).
- [6] T. E. Li, *et al.*, Annu. Rev. Phys. Chem. **73**, 43-71 (2022).
- [7] M. Ruggenthaler, *et al.*, arXiv:2211.04241 [quant-ph] (2022).
- [8] A. Mandal, *et al.*, ChemRxiv [Preprint] (2022). doi: 10.26434/chemrxiv-2022-g9lr7
- [9] S. Zeytinoglu, *et al.*, Phys. Rev. X **7**, 021041 (2017).
- [10] W. Qin, *et al.*, Phys. Rev. Lett. **120**, 093601 (2018).
- [11] C. Leroux, *et al.*, Phys. Rev. Lett. **120**, 093602 (2018).
- [12] S. C. Burd, *et al.*, Nat. Phys. **17**, 898-902 (2021).
- [13] C. Riek, *et al.*, Nature **541**, 376–379 (2017).

Monitoring the progression of virus infection in plants using Raman spectroscopy and principal component analysis

Kaustav Das*, Fawzia Novianti, Ken Komatsu, Terumasa Ito and Kazuhiko Misawa

Tokyo University of Agriculture and Technology, 2-24-16 Nakacho, Koganei, Tokyo 184-8588, Japan

Corresponding author: kdas@go.tuat.ac.jp; +81 42 388 7106

Abstract: Severity of the plant diseases challenging the global food security. Advancement of traditional agricultural technology has become necessary. Here, we present a study to monitor the progression of virus infection in plants using Raman spectroscopy and principal component analysis. Our results presented a gradual spread of infection starting from the low infection level.

1. Introduction

The everlasting effects of contagious plant diseases are posing one of the biggest challenges to global food security along with the increasing demand for food supply and drastic climate change. Among the plant diseases induced from pathogen interaction, virus induced diseases are the most difficult to monitor since they are generally asymptomatic in the initial levels of infections. Conventional methods [1] such as serological and molecular methods are critical in detecting later levels of infections when the infection has become widespread. Such methods lack in monitoring different levels of infections, especially the earliest ones. To provide a proper diagnosis and point of care, monitoring the spread of infections from low to high levels has become necessary. Now, Raman spectroscopy (RS) [2] which provides molecular dynamics in a non-invasive and non-destructive manner, becomes beneficial for obtaining acute spectral signatures related to different levels of infection. Therefore, we present a model study for monitoring the progression of virus infection using RS and principal component analysis (PCA). We used two sets of plants, one being non-infected or healthy set and the other being infected set. Spectra were acquired between 6 to 12 dpi (days post inoculation). By comparing the results (PC score plots) between healthy and infected samples, a gradual characteristic difference was obtained in each dpi with 12dpi being the most distinctive. Such gradual differences between healthy and infected samples led to monitoring the progression of infection in a systematic manner.

2. Methods

We used *Arabidopsis thaliana* plants for this study. The infected set of such plants were inoculated with plantago asiatica mosaic virus. The infected and healthy set of plants were measured using a self-made confocal spontaneous Raman microscope on 6, 9 and 12 dpi. The measured spectra were preprocessed for baseline adjustment and then subjected to PCA. PCA converts the highly correlated variables of spectral data into few uncorrelated variables with maximum variance termed as principal components (PC). Score of such PCs can represent trends between spectral datasets.

3. Results and discussion

Figure 1 shows the PC score plots for healthy and infected samples. PC scores of each dpi presents their individual grouping with group-separation getting larger after 9 dpi. Although both healthy and infected samples exhibited similar trends for each group of PC scores, they seem to differ characteristically when compared directly among the healthy and infected samples. Such difference is relatively smaller in the 6 and 9 dpi, while 12 dpi shows the largest difference. These characteristic differences between healthy and infected samples convey the spreading of infection. Thus, the model study was able to monitor the progression of virus infection, starting from low to high level of infection. Although we were successful in monitoring the spread of virus infection, to detect the presence of virus at the earliest accurately, more robust experimental protocol will be implemented in the future.

4. References

- [1] F. Martinelli *et al.*, *Agron. Sus. Dev.* **35**, 2015.
 [2] C. Farber and D. Korouski, *Anal. Chem.* **90**, 2018.

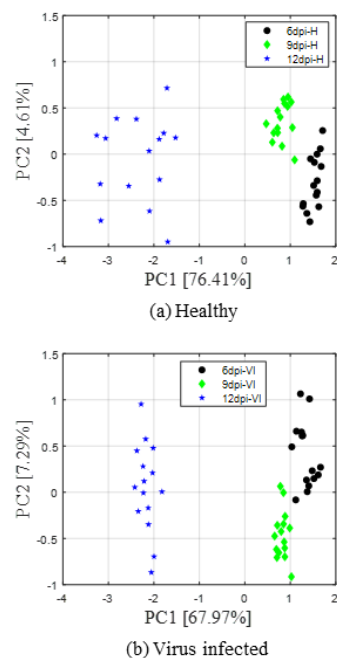


Figure 1 PC score plots

Terahertz Emission from Topological Material SrCd₂Sb₂ single crystals

Po-Wei Gong¹, Yi-Cheng Cheng¹, Pei-Tsung Yang¹, Xin-Yun Chang¹, Jiun-Haw Chu²,
Cheng-Chien Chen³, Jiunn-Yuan Lin⁴, Chih-Wei Luo¹, and Chien-Ming Tu^{1*}

¹Department of Electrophysics, National Yang Ming Chiao Tung University, Hsinchu, 300093 Taiwan

²Department of Physics, University of Washington, Seattle, WA, 98195 USA

³Department of Physics, University of Alabama at Birmingham, Birmingham, AL, 35294 USA

⁴Institute of Physics, National Yang Ming Chiao Tung University, Hsinchu, 300093 Taiwan
e-mail address: cmtu@nycu.edu.tw

Abstract: We report on terahertz emission from topological material SrCd₂Sb₂ single crystals under ultrafast optical excitation with different polarization. Nonzero circular dichroism of the emitted THz radiation were observed as the polarization of optical pulses switch from right circular polarization to left circular polarization. The observed phenomena are coincident with circular photogalvanic effect. Our work demonstrates the potential applications of SrCd₂Sb₂ on opto-spintronics devices.

Introduction

Topological materials (TMs) have attracted much interests both theoretically and experimentally due to their exotic transport phenomena, and potential applications in spintronics. Dirac and Weyl semimetal are quantum matters which its conduction and valance bands cross each other and show linear dispersion around pairs of nodes in reciprocal space. Magnetic Weyl semimetal is bearing seeking for long time, and EuCd₂Sb₂ has been predicted as an ideal magnetic Weyl semimetal. SrCd₂Sb₂, the non-magnetic analogue of EuCd₂Sb₂, has also been predicted to show non-trivial topological phase in room temperature. Besides, THz emission spectroscopy is a powerful contact-free tool to detect the dynamics of photocurrents in topological materials through circular photogalvanic effect [1, 2]. In this study, we report on terahertz emission spectroscopy of SrCd₂Sb₂ single crystals. Significant nonzero circular dichroism of terahertz emission were observed, and this phenomenon agrees with circular photogalvanic effect originated from topological states well.

Results

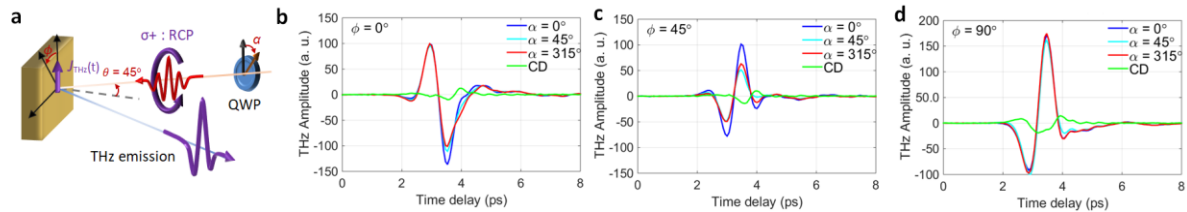


Figure 1. a, circularly polarized optical pulses illuminated a SrCd₂Sb₂ single crystal at an oblique angle $\theta = 45^\circ$ of incidence to generate photocurrents (J_{THz}) with direction perpendicular to the plane of incidence. In b-d, the figures show the emitted THz radiation at different sample orientation of $\phi = 0^\circ, 45^\circ$ and 90° respectively. α : the phase angle of the quarter-wave plate (QWP). The colors represent the polarization of optical pulses: linear- (blue), right-hand-circular- (cyan) and left-hand-circular-polarization (red) for $\alpha = 0^\circ, 45^\circ, 135^\circ$ respectively.

Figure 1 shows the THz waveforms excited by femtosecond optical pulses of different polarization at different sample orientations ϕ . S-wave THz radiation was detected. In-plane contributions to the THz radiation are included only, and the contributions from bulk can be excluded in this scheme. At $\phi = 0^\circ$, as shown in Fig. 1b, significant THz emission was observed under linear polarized (quarter wave-plate phase angle $\alpha = 0^\circ$) optical excitation. As the polarization of optical pulses changed to right-/left-circular polarization ($\alpha = 45^\circ/135^\circ$), similar THz wave-forms were observed, and the polarity of the THz wave did not change also. However, nonzero THz emission circular dichroism can be observed. Interestingly, the polarity of the all THz emission circular dichroism show the same polarity, and it indicates the spin-polarized photocurrents keep their direction under the rotation of samples along sample's surface normal. These phenomena are coincident with circular photogalvanic effect-the spin-polarized photocurrent originated from topological states of TMs.

[1] N. Sirica, *et al.*, "Tracking Ultrafast Photocurrents in the Weyl Semimetal TaAs Using THz Emission Spectroscopy," *Phys. Rev. Lett.* **22**, 197401 (2019).

[2] L. Luo, *et al.*, "A light-induced phononic symmetry switch and giant dissipationless topological photocurrent in ZrTe₅," *Nat. Mat.* **20**, 329, (2021).

Initial reaction dynamics of a red fluorescent protein TagRFP under mutation of S158T observed by 10fs visible laser pulse

^ANational Yang-Ming Chiao-Tung Univ., ^BKanagawa Univ., ^CJILA-University of Colorado Boulder

Atsushi Yabushita^{A,B}, QiuJun Lin^A, Ying Kuan Ko^A, Takayoshi Kobayashi^A, Izumi Iwakura^B, Ralph Jimenez^C

In the field of bioimaging, fluorescent proteins (FPs) emitting different colors are used to observe various components in a single shot taking the image in full color. TagRFP is one of FPs emitting red color whose photostability is known to be improved by mutation of S158T [1]. The improvement is thought to be related with a reactivation process which only appears in the mutant [2], however its mechanism is still not clear.

We have observed ultrafast dynamics of the original TagRFP and its mutant to visualize the difference in their primary photoreaction. The pulse duration of the 10fs visible pulse laser could visualize the vibrational dynamics simultaneously observing electronic dynamics. The mechanism which causes the difference was well explained by comparing the result with quantum chemical calculation.

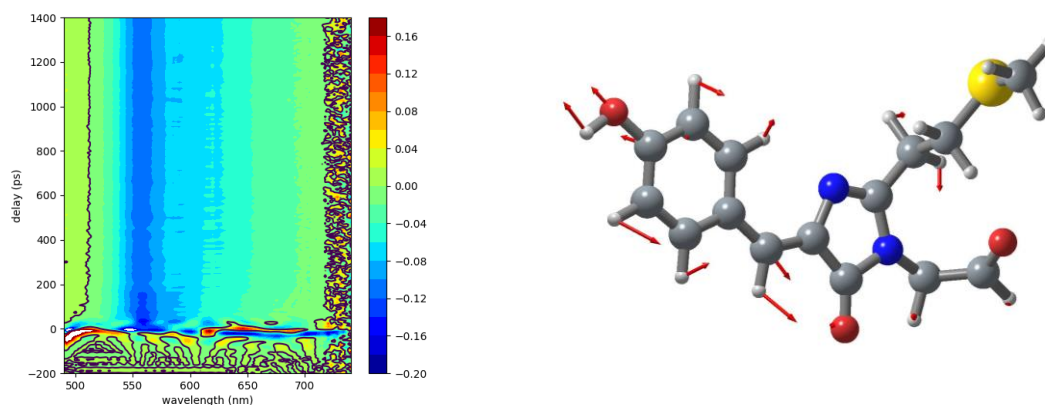


Fig. 1 (Left) Two dimensional view of the measured transient absorption spectra and (Right) Calculated vibrational mode corresponding to the difference appearing on mutation.

[1] Nathan C Shaner, Michael Z Lin, Michael R McKeown, Paul A Steinbach, Kristin L Hazelwood, Michael W Davidson & Roger Y Tsien, “Improving the photostability of bright monomeric orange and red fluorescent proteins”, *Nature Methods*, 5, 545-551 (2008)

[2] Rui Liu, Qing-Nan Liang, Shu-Qi Du, Xiao-Jian Hu, Yu Ding, “The crystal structure of red fluorescent protein TagRFP-T reveals the mechanism of its superior photostability”, *Biochem Biophys Res. Commun.*, 477 (2):229-234 (2016)

Nematic ultrafast dynamics in SnS crystals

Nguyen Nhat Quyen¹, Tz-Ju Hong¹, Chin En Hsu², Wen-Yen Tzeng¹, Chien-Ming Tu¹, Chia-Nung Kuo^{3,4}, Hung-Chung Hsueh^{2,5}, Chin-San Lue^{3,4}, **Chih-Wei Luo**^{1,4,6,7}

¹ Department of Electrophysics, National Yang Ming Chiao Tung University, Hsinchu 30010, Taiwan

² Department of Physics, Tamkang University, New Taipei City 251301, Taiwan

³ Department of Physics, National Cheng Kung University, Tainan 70101, Taiwan

⁴ Taiwan Consortium of Emergent Crystalline Materials, Ministry of Science and Technology, Taipei 10601, Taiwan

⁵ Research Center of X-ray Science, College of Science, Tamkang University, New Taipei City 251301, Taiwan

⁶ National Synchrotron Radiation Research Center, Hsinchu, 30076, Taiwan

⁷ Institute of Physics, National Yang Ming Chiao Tung University, Hsinchu, 30010, Taiwan

Abstract: This study determines the nematic ultrafast dynamics of photoexcited electrons and phonons in SnS single crystals using polarization-dependent femtosecond spectroscopy at various temperatures. Besides the fast relaxation of photoexcited electrons, a damped oscillation component with a frequency of 36~41 GHz is also present in transient reflectivity change ($\Delta R/R$) spectra generated by the thermoelastic effect. The results of this study show that electrons and coherent acoustic phonons demonstrate significant anisotropy on the ac-plane in the transition region from 330 K to 430 K, possibly because of strong electron-phonon coupling. These are essential in anisotropic heat dissipation and charge carrier mobility in polarization-sensitive optical and optoelectronic devices.

1. Introduction

New classes of two-dimensional (2D) materials beyond graphenes, such as transition metal dichalcogenides (TMDCs) and black phosphorus, have significant physical/chemical properties and many potential applications. Since the highly symmetrical crystal structure, graphene and most TMDCs feature in-plane isotropic characteristics. However, some 2D materials, such as black phosphorus and the bulk orthorhombic group IV-VI compounds of SnS, SnSe, GeS, and GeSe, exhibit significant in-plane anisotropic properties and have a low lattice symmetry. Similarly to black phosphorus, SnS is a layered material with anisotropic electronic properties and good environmental, thermal, and dynamic stability. However, there is no study on the ultrafast dynamic responses and acoustic phonons in SnS, particularly the evolution of electronic and phononic anisotropies.

2. Results and discussion

Figure 1(a) shows the crystal structure of SnS and schematics of the polarized pump-probe measurements [1]. The grey and yellow balls represent Sn and S atoms, respectively. The $\Delta R/R$ was measured using a dual-color pump-probe system (400 nm/3.1 eV pump, 800 nm/1.55 eV probe) and the standard lock-in technique with a femtosecond Ti:sapphire laser as the light source for the excitation pulses (a pulse duration of 70 fs and a repetition rate of 5.2 MHz). The respective fluences of the pump and probe beams were 73.2 $\mu\text{J}/\text{cm}^2$ and 5.5 $\mu\text{J}/\text{cm}^2$. As shown by Fig. 1(b), the typical $\Delta R/R$ along the *a*-axis of SnS at 300 K with the fitting of an $\Delta R/R = A_1 e^{-t/\tau_1} + A_2 e^{-t/\tau_2} + A_3 e^{-t/\tau_3} \dots$ Eq. (1). The solid line is the sum of the dashed lines. The inset shows the oscillation component of $\Delta R/R$ when the decaying background is subtracted, and the curve is fitted using a cosine function (solid line). Fig. 1(c) shows the orientation-dependent $\Delta R/R$ for an SnS single crystal, from $\theta_{\text{probe}} = 0^\circ$ (zigzag direction) to 90° (armchair direction) at 300 K. The results of this study show that electrons and coherent acoustic phonons demonstrate significant anisotropy on the ac-plane. For the details of this study, please refer to Ref. [1].

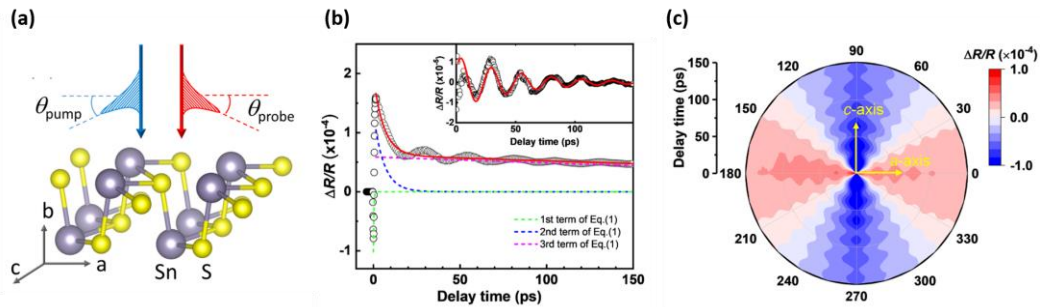


Fig. 1. The nematic dynamics of photoexcited electrons and phonons in SnS single crystals are revealed using polarization-dependent femtosecond spectroscopy.

3. References

[1] Nguyen Nhat Quyen et al., "Nematic electron and phonon dynamics in SnS crystals," *App. Phys. Lett.* **121**, 172105 (2022).

Recording and batch decoding of SQAM signal for Holographic memory

Satoshi Honma, Hironori Ito,

University of Yamanashi, 4-3-11, Takeda, Kofu, Yamanashi, 400-8511, Japan
shonma@yamanashi.ac.jp

Abstract: Recording scheme of a spatial quadrature amplitude modulated (SQAM) signal is expected to improve the recording density of the holographic data storage (HDS). The problem is to realize this with simple optics. In this report, we explain our concept of the interleaved phase method to generate the SQAM signal and of the batch decoding technique of the reproduced signal with simple optical constructions.

1. Introduction

It is expected that HDS will be developed as the next generation optical memory. A recording scheme of a SQAM signal is a promising technique to achieve high recording density of the HDS. It is important to design a simple optical system for the generation of the SQAM signal and the phase measurement of the reproduced signal. We have proposed the interleaved phase method to generate the SQAM signal with a spatial phase modulator. We are also currently investigating a phase detection method by simultaneously reproducing of SQAM signals using HDS optics as an optical interferometer. We introduce the concept of the systems.

2. Interleaved phase method for generation of SQAM signal

Fig. 1 shows the recording process of the SQAM signal in the HDS with the interleaved phase method. To generate the SQAM signal of $A_{x,y} \exp j\varphi_{x,y}$, we calculate the phase distribution for the spatial phase modulator given by

$$\theta_{n,m} = \varphi_{x,y} + (-1)^{n+m} \arccos(1 - A_{x,y}) \quad (1)$$

, where $\varphi_{x,y}$ and $A_{x,y}$ are phase and amplitude of the SQAM signal at coordinates (x,y) of the symbol, n, m are the horizontal and vertical pixel coordinates of the spatial phase modulator. $c \times c$ pixels are used to represent one symbol of the SQAM signal, where in general c is generally 8. The phase-modulated light, whose phase value is $\theta_{n,m}$ by the spatial modulator, is passed through the spatial low-frequency filter optics to remove unwanted components, resulting in the final SQAM signal of $A_{x,y} \exp j\varphi_{x,y}$.

3. Bath reading and decoding (BRD) of SQAM signal

Fig. 2 shows the conceptual diagram of the BRD. Three SQAM signals are simultaneously reproduced from holograms recorded at different positions by irradiating multiple reading beams. Since the signal beams are incident to the camera at different angles, interference fringe patterns with multiple different spatial frequencies are formed according to the angular difference between the beams. The complex amplitude distributions of the i -th SQAM signals is defined by $C_i = A_i \exp j\varphi_i$ ($i = 0, 1, 2$). From the spatial frequency difference, the distribution corresponding to $C_1 C_0^*$ and $C_2 C_0^*$ can be extracted using Fourier analysis, where the asterisk indicates the conjugated phase. Assuming that only SQAM signal distribution C_0 is known in advance, by dividing C_0^* from the above distribution, the distributions C_1 and C_2 can be decoded. Fig. 3 shows the analytical result of the decoded signals by BRD. The decoding is confirmed to be relatively accurate, although distortions occur near the pixel boundaries.

4. Conclusion

We have presented our proposed method of recording an SQAM signal in a holographic memory and decoding the complex amplitude value of the reproduced signal using a simple optical system.

5. References

- [1] S. Honma, T. Sekiguchi, "Multilevel phase and amplitude modulation method for holographic memories with programmable phase modulator", *Opt. Rev.* Vol. 21, pp. 597–598 (2014)
- [2] J. Igarashi, H. Ito, S. Honma, "Batch recording of multiple SQAM signal and self-reference detection technique", *Opt. Rev.*, online (2023).

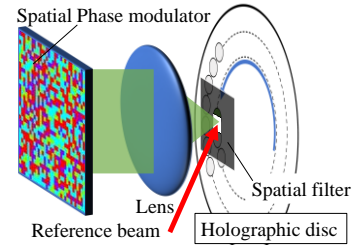


Fig. 1 Recording process

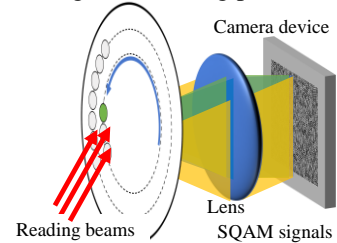


Fig. 2 Batch reading process

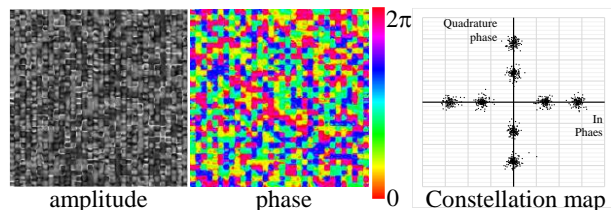


Fig. 3 Decoded SQAM signal

Pulse shaping for 3-dimensional integration of kinetic energy via light

Hironori Ito, Yuki Uchiyama and Satoshi Honma

University of Yamanashi, 4-3-11, Takeda, Kofu, Yamanashi, 400-8511, Japan
hito@yamanashi.ac.jp

Abstract: This study is to challenge how efficiently pulse shapes can be used to convert kinetic energy into liquid kinetic energy. This is fundamental study of pulse shaping to match the temporally changing solvent state to achieve the minimum entropy state that generates the maximum amount of work. The energy dense state of the liquid is converted into fluid kinetic energy through cycles of bubble formation and contraction. Introduce a new concept of 3-dimensional integration of kinetic energy to fields such as biomedicine and robotics by improving the efficiency of light-kinetic energy conversion and expanding its applicability.

1. Introduction

The generation of bubbles by irradiating a liquid with a femtosecond pulsed laser (fs laser) has attracted attention as a phenomenon for distributing kinetic energy with high spatial resolution on the micrometer scale. [1,2] Even though the fundamental wave is not absorbed in water, at the fs laser focal point, the generation and contraction of bubbles is accompanied by the generation of plasma due to multi-photon absorption. The bubble expansion-contraction cycle powers fluid pumping and actuators. Especially in microfluidic devices, where wiring is considered difficult, distributing optical energy to any desired position in three-dimensional space enables systematic operation of integrated power sources, as shown in Fig. 1. Despite the strong desire for such a prospect, current research on laser-induced bubbles is focused on processing and analysis and lacks a measure of optical-kinetic energy conversion efficiency.

2. Plan to improve energy conversion efficiency with pulse shaping

For minimum entropy, as many photons as possible must be used to excite electrons in a limited space. The pulse waveform is optimized based on the density of the electronic state of the liquid and the wavefront at the focal point. In order to clarify the achievement of kinetic energy conversion of liquid by pulse shape, (1) an observation system for bubbles generated by laser will be constructed, and (2) the kinetic energy is evaluated from the flow velocity of the liquid and feedback is provided to the parameters of pulse shape.

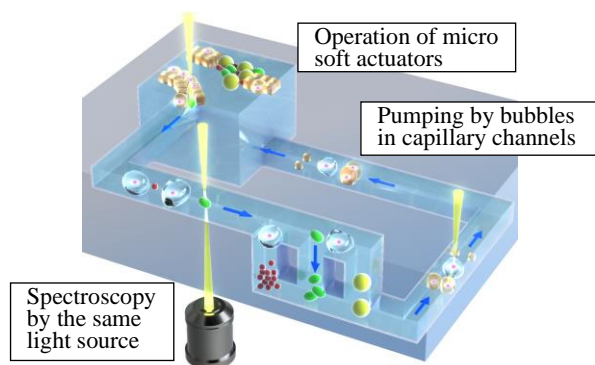


Fig. 1 Systematic applications realized by 3D kinetic-energy integration by light such as microfluidic devices

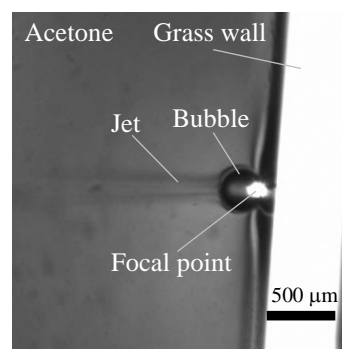


Fig. 2 CMOS Image of microjet from laser induced bubbles

3. Preliminary experiments on bubble generation by laser

The optical cell was filled with acetone and a femtosecond laser pulse was focused on the methyl-elo deposit on the wall surface. A strong microjet was observed with the generation of bubbles as shown in Fig. 2. This phenomenon is known to be caused by the Marangoni effect due to the temperature gradient at the gas-liquid interface and the expansion and contraction cycle of bubbles. This jet enables visualization of momentum, which can be used to evaluate energy conversion efficiency.

4. Conclusion

Improvement of optical-kinetic energy conversion efficiency by pulse shaping is proposed. This research will lead to medical and industrial applications through three-dimensional integration of kinetic energy using light.

5. References

[1] Y. Tagawa et.al., *Physical Review X* **2** 031002 (2012). [2] Y. Hosono et.al., *JJSP* **84** 11 (2018).

Detection of structural changes in DNA due to methylation using Raman spectroscopy

Haruki Kanae and Kazuhiko Misawa

Department of Biomedical Engineering, Tokyo University of Agriculture and Technology, 2-24-16 Naka-cho, Koganei, Tokyo, Japan
Author e-mail address: s233092t@st.go.tuat.ac.jp

Abstract: DNA methylation regulates transcription, and its aberration is one of the causes of cancer. Previous studies have suggested that DNA methylation has some effect on DNA conformational changes. However, detailed structural information has not been obtained. In this study, we investigated the structural changes in DNA caused by methylation using Raman spectroscopy (RS).

1. Introduction

Cancer is one of the common causes of death in the world. If the detection of it gets delayed, the rate of survival decreases and the burden of treatment increases. Therefore, early detection is essential. Loss of normal transcriptional regulation by abnormal deoxyribonucleic acid (DNA) causes cancer. General cancer detection techniques include imaging and tumor marker; however, these methods can only detect cancer after it has progressed to a certain stage. For earlier detection, it is required to accurately detect DNA abnormalities that led to cancer.

DNA methylation is one of the mechanisms that regulate DNA transcription and such abnormalities have already been identified in many cancer patients. However, it is not clear how DNA methylation affects transcriptional regulation. Tsukakoshi et al. [1] demonstrated that the binding activity of DNA oligonucleotides derived from gene promoter regions to a transcription factor is altered by methylation. This suggested that the conformational change caused by methylation may affect transcriptional regulation. In the previous works, circular dichroism (CD) spectra were measured to analyze the effects of methylation on the DNA structures, however, CD does not provide detailed structural information.

In this study we use Raman spectroscopy (RS) to detect conformational changes in DNA induced by methylation. Since RS generates vibrational information of molecules, it allows us to identify structural modifications of DNAs [2]. With this method, we elucidate the transcriptional regulatory mechanism of DNA methylation by investigating how structural differences determined by RS affect transcriptional regulation.

2. Method

To observe the structural changes caused by methylation, Raman measurements were performed on DNA differing only in the presence or absence of methylation. The samples measured were methylated and unmethylated Hras1. Hras1 is an oncogene that produces the RAS protein, which is responsible for intracellular signaling that promotes cell multiplication.

3. Results and Discussion

Figure 1 shows the Raman spectra of methylated and unmethylated Hras1. These differences in spectra reflect only differences due to methyl groups and differences in DNA structure. The spectra confirmed the spectral changes associated with the conformational changes of DNA. In the future, we will investigate how the conformational differences affect transcriptional regulation to elucidate the transcriptional regulatory mechanism of DNA methylation.

References

- [1] K. Tsukakoshi, S. Saito, W. Yoshida, S. Goto, K. Ikebukuro, "CpG Methylation Changes G-Quadruplex Structures Derived from Gene Promoters and Interaction with VEGF and SP1," *Molecules* 23, 944 (2018).
- [2] J. Palacký, P. Mojžeš, I. Kejnovská, M. Vorlíčková, "Does Raman spectroscopy recognize different G-quadruplex arrangements?" *J. Raman Spectrosc.* 51, 301–312 (2020).

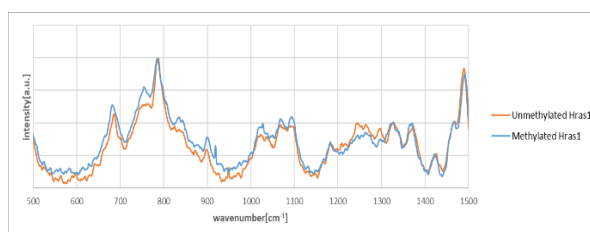


Fig.1 Raman spectra of methylated and unmethylated Hras1

Toward Discovery of Biomarkers for New Diagnostic Techniques of IgA Nephropathy

Daichi Igarashi, Terumasa Ito, Daisuke Yoshino, and Kazuhiko Misawa

Tokyo University of Agriculture and Technology, 2-24-16 Naka-cho, Koganei, Tokyo 184-8588, Japan
s231086s@st.go.tuat.ac.jp

Abstract: Kidney biopsy is used for definitive diagnosis of IgA nephropathy, but its invasive nature is a challenge. Although minimally invasive diagnostic techniques have been developed, none of them have been put into practical use. This study aims to create a kidney model that can reproduce IgA nephropathy, which is necessary for the discovery of biomarkers that can lead to the development of minimally invasive diagnostic techniques.

Introduction

The kidneys have a filtration function by excreting and reabsorbing substances in the body. IgA nephropathy is one of the intractable diseases and may progress to kidney failure. In this disease, IgA, one of the immune antibodies, becomes abnormal for some reason and deposits in kidney cells. This leads to inflammation of the glomerulus and impairs the filtration function [1].

In Japan, kidney biopsy, in which kidney tissue is collected, is currently used for definitive diagnosis, but it is highly invasive and places a heavy burden on patients. A minimally invasive diagnostic method using Gd-IgA, one of the abnormal IgA, as a biomarker and measuring its amount in the patient's serum was developed [2]. However, because healthy individuals likely to have Gd-IgA and the amount of Gd-IgA varies among individuals, it is difficult to distinguish between healthy individuals and patients; thus, the accuracy of diagnosis is low.

This study aims to help researchers search for biomarkers that specifically occur after glomerular inflammation to develop new diagnostic techniques to distinguish IgA nephropathy patients from healthy controls in a minimally invasive manner. However, in general, the search for biomarkers requires the use of biological samples such as tissue or blood derived from patients. In such studies, it is also necessary to manipulate the presence or absence of inflammation and make comparisons. Recently, attention has been focused on modeling kidney disease using kidney organoids. In this work, as the first step, we create a kidney model that can reproduce IgA nephropathy.

The experimental plan toward the creation of a kidney model is outlined as follows. To reproduce the pathogenesis principle of IgA nephropathy as described above, the kidney model uses co-culturing of both kidney cells and glomerular models. In addition, it is necessary for the model to reproduce the inflammation that is caused by aberrant IgA. Therefore, we first test multimeric IgA, a type of aberrant IgA, to check whether it can cause inflammation. The kidney cells are cultured in the medium mixed with the multimeric IgA to determine the presence or absence of cellular inflammation. Once the inflammation is confirmed, we plan to create a more realistic kidney model with co-culturing of kidney cells together with a glomerular model, where the presence or absence of inflammation is again determined. Finally, we will also examine whether the tissue degeneration characteristic of IgA nephropathy is reproduced.

Currently, using kidney cells cultured in medium mixed with multimeric IgA, we are testing immunofluorescent antibody methods to confirm whether multimeric IgA is deposited on the cells and to confirm the distribution of the deposited multimeric IgA. In this presentation, I will talk about the current progress of the experiment.

References

- [1] Suzuki, Hitoshi, et al., "The pathophysiology of IgA nephropathy," *Journal of the American Society of Nephrology* **22**, 10, 1795 (2011).
- [2] Bagchi, Soumita, et al. "Significance of serum galactose deficient IgA1 as a potential biomarker for IgA nephropathy: A case control study," *PLoS One* **14**, 3, e0214256 (2019).

Suppression of the Tailing Effect for Pathogen Inactivation with UVC Ultrashort Pulsed Light

Shundai Yamamoto^A, Hideki Abe^B and Kazuhiko Misawa^A

^ADepartment of Applied Physics, Tokyo University of Agriculture and Technology, 2-24-16 Naka-cho, Koganei, Tokyo, Japan
^BResearch and Development Department, Central Blood Institute, Japanese Red Cross Society, Tatsumi 2-1-67, Koto-ku, Tokyo, Japan
 Author e-mail address: s226963q@st.go.tuat.ac.jp

Abstract: In the inactivation of pathogens by ultraviolet light, the inactivation rate has been reported to decrease with increasing irradiation dose, which is commonly known as the tailing effect (TE). In this study, we compared the inactivation effects between CW-LED and femtosecond pulsed laser for developing a new method to suppress TE. We found that femtosecond pulsed lasers suppressed TE and inactivated pathogens by more than one order of magnitude in comparison with CW-LED. The results of this study provide a new method for the practical application of bacterial inactivation by ultraviolet light.

1. Introduction

The spread of contagious infections has increased the demand for technologies to inactivate pathogens by ultraviolet (UV) irradiation. UVC (200-280nm) light inactivates pathogens by denaturing the nucleic acids by direct absorption, without the aid of chemical components. The inactivation kinetics of UV light follows logarithmic decay model if the inactivation rate is constant. However, experimentally, the assumption of a constant inactivation rate breaks down. Previous studies have shown that the inactivation rate decreases with increasing irradiation dose, which is commonly known as the tailing effect (TE). One such study reported that TE occurs under UV inactivation in phosphate buffer solution (PBS) with pathogen aggregation and suggested that TE may originate from light shielding effects and/or photo-reactivation [1]. Despite the advances in understanding the mechanism, there are few reports on how to suppress TE. In this study, we propose a new irradiation method using ultrashort pulsed light (UPL) in the UVC region to suppress TE. A CW-LED and a femtosecond (fs) pulsed laser were irradiated to bacterial solution, and their survival rates were compared.

2. Methods

E. coli (NBRC 3301) was suspended in PBS and the viable bacteria concentration of the bacterial solution was adjusted to 10^8 CFU /mL (CFU: colony forming unit). 100 μ L of the suspension was then sealed in a 1 mm optical path length quartz cell with a magnetic stirrer. An LED with a center wavelength of 268 nm and a spectral width of 11 nm was used as the continuous light source. The pulse source was a fs pulsed laser with a center wavelength of 800 nm, repetition rate of 10 kHz, pulse energy of 0.5mJ and pulse width of 40 fs. The light was then converted to pulsed light with a center wavelength of 268 nm and a spectral width of 2.1 nm using third harmonic generation. Peak power of fs pulse had approximately 8 orders of magnitude higher than that of LED. As the fs pulsed laser has a Gaussian spatial intensity distribution, a diffuser was installed in front of the irradiated sample to ensure a uniform intensity distribution on the irradiated surface. Also, a 10 mm square aperture mask was placed in front of the sample for both lights. The irradiation dose was calculated as the product of average power and irradiation time; the average power was set to be at 1.0 mW/cm² for both lights. The bacterial inactivation effect was assessed using bacterial survival counts by microscopic observation. All samples were diluted in PBS, applied to LB agar medium and incubated at 35°C for 24 hours. The bacterial survival rate was calculated from dividing the number of bacterial colonies before and after light irradiation.

3. Results and Discussion

The results of the bacterial inactivation effects are shown in Fig. 1. We found that the CW-LED exhibited TE and produced inactivation less than 4 orders of magnitude at 700 mJ/cm², whereas the UPL suppressed TE and inactivated the pathogen over 5 orders of magnitude at the same irradiation dose. We are currently carrying out microscopic observations to examine the formation of pathogen aggregation under continuous and pulsed light irradiation.

Reference:

[1] Eirini Vitzilaiou, Asaph M. Kuria, Henrik Siegmundfeldt, Morten A. Rasmussen, Susanne Knøchel, The impact of bacterial cell aggregation on UV inactivation kinetics, *Water Research* **204**, 117593 (2021).

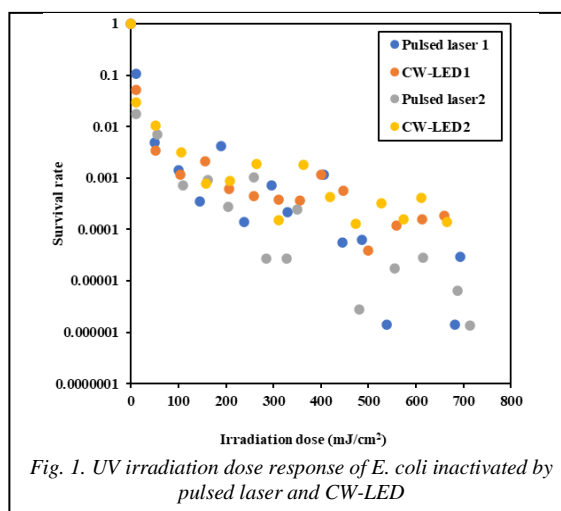


Fig. 1. UV irradiation dose response of *E. coli* inactivated by pulsed laser and CW-LED

Acquisition of Raman Spectra of Foamed Macrophages for Early Diagnosis of Atherosclerosis

Kohei Eguchi*, Terumasa Ito, Daisuke Yoshino and Kazuhiko Misawa

Tokyo University of Agriculture and Technology, 2-24-16 Naka-cho, Koganei, Tokyo 184-8588, Japan
*s234206t@st.go.tuat.ac.jp

Abstract: Current diagnosis of atherosclerosis is made after plaque formation, which can lead to vascular disease. In this study, we will use Raman microscopy to investigate substances that may serve as markers for early diagnosis of atherosclerosis in macrophage foam formation, foam cell accumulation, and plaque formation.

Arteriosclerosis is a general term for a disease in which plaque and thrombi form on arterial walls due to the deposition of cholesterol and other substances, resulting in hardening and loss of elasticity of the arterial walls, making blood vessels more likely to become clogged. In particular, atherosclerosis is the most common form of arteriosclerosis, and diseases such as myocardial infarction, angina pectoris, and stroke associated with atherosclerosis are the leading causes of death worldwide [1].

Plaques in atherosclerosis are formed as shown in Figure 1. First, low density lipoprotein (LDL), a type of cholesterol, enters the vascular endothelium from the artery and is oxidized ((1) in Fig. 1). Then, macrophages in the vascular endothelium take up the oxidized LDL ((2) in Fig. 1) and form foam cells filled with lipid droplets ((3) in Fig. 1). When foam cells accumulate, they form plaques ((4) in Fig. 1). When this plaque ruptures, deposits within the plaque leak into the bloodstream, causing thrombus formation and vascular occlusion, which may induce myocardial infarction or angina pectoris [2]. Currently, the most common diagnostic methods for atherosclerosis are MRI and CT angiography to examine the narrowing of blood vessels and changes in blood flow caused by plaques formed on the arterial wall. These tests can diagnose plaques with a particularly high risk of rupture, but these methods cannot be used unless the plaques are formed to an observable size. Therefore, it is important to establish a technique to observe the early stages of macrophage accumulation (i.e. early stages of plaque formation) for early diagnosis of atherosclerosis.

Stiebing et al. observed the uptake of oxidized LDL by macrophages using Raman spectroscopy, which is particularly easy to discriminate lipids due to differences in molecular vibration [3]. As a result, they found Raman bands of β -carotene specific to the lipid portion of macrophages that took up oxidized LDL. However, the detection of β -carotene does not indicate macrophage foaming. Early diagnosis of atherosclerosis requires direct detection of changes in components and molecular structures involved in foam cell formation and accumulation that lead to plaque formation.

In this study, we propose to use Raman spectroscopy to investigate not only the uptake of oxidized LDL by macrophages, but also possible markers of atherosclerosis in macrophage foaming, foam cell accumulation, and plaque formation for early diagnosis of atherosclerosis. As the first step, LDL is oxidized and then incubated with macrophages to allow the macrophages to take up the oxidized LDL, and spontaneous Raman microscopy is used to observe whether the macrophages have taken up the oxidized LDL and whether the macrophages are bubbled. This presentation will describe the experimental technique in detail and the progress of the study.

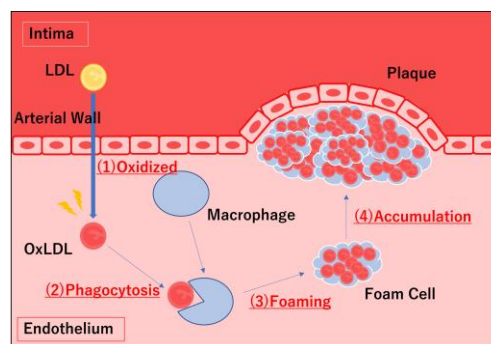


Figure 1. Schematic representation of the progression of the atherosclerosis

[1]World Health Organization, “Cardiovascular diseases”, 2021.

[2]Ross R, “The pathogenesis of atherosclerosis: a perspective for the 1990s”, Nature, 29;362(6423), pp.801-809(2003).

[3]Clara Stiebing, et.al, “Raman imaging of macrophages incubated with triglyceride-enriched oxLDL visualizes translocation of lipids between endocytic vesicles and lipid droplets”, JOURNAL OF LIPID RESEARCH, Vol. 58, Issue 5, pp.876-883(2017).

Transdermal Penetration of Self-Dissolving Microneedles Using Coherent Raman Scattering Microscopy

Yuki Sekiya and Terumasa Ito

Department of Biomedical Engineering, Tokyo University of Agriculture and Technology, 2-24-16 Naka-cho, Koganei, Tokyo, Japan
Author e-mail address: s208239q@st.go.tuat.ac.jp

Abstract: Self-dissolving microneedles hold promise as a novel drug delivery approach. However, conventional analytical approaches lack the ability to measure real-time drug penetration through the skin. We present a transdermal penetration measurement of low-molecular-weight drugs in dissolvable microneedles using coherent Raman scattering microscopy. This non-labeled and real-time drug measurement will contribute significantly towards evaluating the effectiveness of medical MNs and advancing their practical use.

The epidermis possesses a barrier function against water and external stimuli. To achieve transdermal drug delivery, it is essential to allow drug penetration through this epidermal barrier without disrupting it. Microneedles (MNs) have garnered attention as a novel transdermal drug delivery system to facilitate efficient drug absorption through the epidermis. Conventional approaches have utilized metal or silicon-based MNs for transdermal administration, involving drug coating on the MN surface or drug encapsulation within the MN structure for release in the skin. However, these methods present drawbacks like the risk of needle breakage upon application, potentially leaving residual fragments in the skin, which compromises safety.

Recently, interest has shifted towards self-dissolving MNs crafted from materials with high biocompatibility and safety, where the needles dissolve upon application without leaving residues. This mechanism relies on the dissolution of needles within the skin's moisture, facilitating drug release. While self-dissolving MNs hold promise as a novel drug delivery approach, they have yet to be fully realized as pharmaceutical products, necessitating further research. Specifically, there is a need to establish effective evaluation methods, especially concerning drug permeability assessment, which could enhance our understanding of the efficacy of self-dissolving MNs. For instance, Katsumi et al. [1] has investigated self-dissolving MNs utilizing a low-molecular-weight drug alendronate (ALN), which is used for treating osteoporosis. Their assessment includes *in vitro* ALN release from MNs, time-dependent dissolution observation via microscopy, microscopy-based characterization of rat skin penetration, and ALN plasma concentration measurements. However, such approaches lack the ability to measure real-time drug penetration through the skin.

Here, we propose a new approach utilizing coherent Raman scattering microscopy [2] to evaluate the skin permeability of low-molecular-weight drugs delivered by MNs. Coherent Raman scattering microscopy allows real-time permeability assessment of low-molecular-weight drugs without requiring labeling, which can be employed to measure the depth and time of drug penetration within skin tissue [3]. In this study, we will focus on the spatiotemporal kinetics of common low-molecular-weight drugs, such as migraine medications and anesthetics, released from the applied MNs. This non-labeled and real-time drug measurement will contribute significantly towards evaluating the effectiveness of medical MNs and advancing their practical use.

References:

- [1] H. Katsumi, Y. Tanaka, K. Hitomi, S. Liu, Y.-S. Quan, F. Kamiyama, T. Sakane and A. Yamamoto, "Efficient Transdermal Delivery of Alendronate, a Nitrogen-Containing Bisphosphonate, Using Tip-Loaded Self-Dissolving Microneedle Arrays for the Treatment of Osteoporosis," *Pharmaceutics* **9**, 29 (2017).
- [2] J. X. Cheng and X. S. Xie, *Coherent Raman Scattering Microscopy* (CRC Press, 2013).
- [3] T. Ito, R. Iguchi, F. Matsuoka, Y. Nishi, T. Ogihara, and K. Misawa, "Label-Free Skin Penetration Analysis Using Time-Resolved, Phase-Modulated Stimulated Raman Scattering Microscopy," *Biomed. Opt. Express* **12**, 6545-6557 (2021).

Electrolysis measurements and evaluation of boron-doped diamond-coated electrode materials for fuel cells

Yu Okano ^A, Ken Okano ^B and Kazuhiko Misawa ^A

^A Department of Applied Physics, Tokyo University of Agriculture and Technology, 2-24-16 Naka-cho, Koganei, Tokyo, Japan

^B Department of Material Science, International Christian University, 3-10-2 Osawa, Mitaka-shi, Tokyo 181-8585, Japan

Author e-mail address: s197660t@st.go.tuat.ac.jp

Abstract: In this study, an alternative electrode material for fuel cells was prepared by coating conductive boron-doped diamond (BDD) on the surface of a graphite substrate. The performance was confirmed by electrolysis and evaluated by Raman measurements and SEM observations before and after electrolysis. The graphite electrode surface was etched after prolonged electrolysis, while negligible change was observed in the BDD-coated sample. This suggests that the BDD coating is useful as an electrode for fuel cells.

1. Introduction

Batteries, especially fuel cells, are essential for the effective use of renewable energy to solve global energy problems. Various technologies are being developed for the practical application of fuel cells, among which the development of electrodes with high reaction efficiency and corrosion resistance is very important. Platinum and platinum group electrodes are attracting attention because of their high exchange current density, but these are rare metals and will not lead to the sustainable spread of fuel cells. Therefore, electrodes made from carbon, which are abundant on earth, are attracting attention as an alternative to platinum-based electrodes. Carbon has a variety of allotropes, including the highly conductive but chemically unstable graphite and the generally less conductive but chemically stable diamond. Previous reports have shown that boron doping of diamond (BDD) lowers its intrinsic resistance to around 10^{-3} [Ω -cm] [1]. However, bulk BDD alone cannot be used as an electrode due to its relatively high resistance. In this study, we attempted to develop an electrode that utilizes the electrical conductivity of graphite and the surface stability of diamond by coating a BDD film on the surface of graphite by vapor-phase growth.

2. Methods

The samples prepared are pure graphite rods (resistance 2 [Ω]) coated with BDD doped with boron trioxide (B_2O_3), where the boron doping to carbon in the BDD is 99:1 ($R=1900$ [Ω]). The reference sample is a pure graphite rod. The electrical properties of the samples were measured by cyclic voltammetry (CV) [2,3]. In this measurement, the redox reaction at the electrode surface can be assessed from the voltage-current characteristic. To determine the durability of the samples in the redox reaction, long-term electrolytic measurements were carried out at a sweep rate of 4 V/s for 185 hours. Crystallinity and surface uniformity of the graphite were measured non-destructively using a Raman microscope as part of the evaluation of the sample electrodes before and after CV, and the surface condition was also confirmed using a scanning electron microscope.

3. Results and Discussion

For the graphite sample, the electrolysis results are shown on the left side of Fig. 1 where the current level decreases after 185 hours (Purple line). SEM observation of the surface before and after electrolysis (Fig. 2 upper panel) showed the surface roughness after electrolysis. Raman spectral results before and after CV are shown in Fig. 3. From these Raman spectra, the crystallinity of the graphite sample can be characterized by the D-band (1360 cm^{-1})/G-band (1580 cm^{-1}) intensity ratio. The D-band/G-band ratio before CV was 0.334 (blue line) and the ratio after the CV measurement was 0.165 (light blue line) where a lower D-band/G-band ratio corresponds to a better crystallinity. This result indicates that the electrolysis over a long period of time etched away the less crystalline parts of the graphite surface, leaving only the more crystalline parts.

The results of the electrolytic measurements of the BDD samples (right-hand side of Fig. 1) showed no significant degradation in the redox reaction after 185 hours. Surface observations by SEM before and after electrolysis showed no exfoliation (lower part of Fig. 2). The Raman spectra shows a characteristic peak of diamond at 1332 cm^{-1} . Negligible change was found in the Raman spectra between before (red line in Fig. 3) and after (pink line) electrolysis. From the higher durability of BDD-coated samples, we concluded that diamond coating is useful as an electrode in fuel cells.

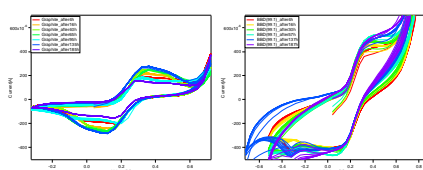


Fig. 1: CV experiment results

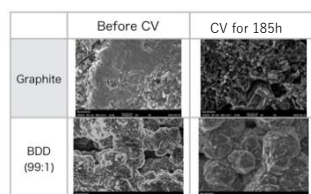


Fig. 2: Results of surface observations by SEM

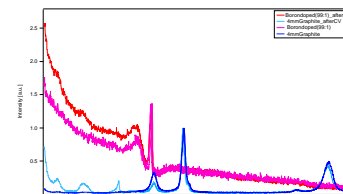


Fig. 3: Raman measurements results

References

- [1] K. Okano *et al.*, "Synthesis of diamond thin films having semiconductive properties" *Jpn. J. Appl. Phys.* 27, pp. L173-175(1988)
- [2] "Denki Kagaku Sokutei Manyuru Kiso." (in Japanese) The Electrochemical Society of Japan, ed., (2002)
- [3] Noémie Elgrishi *et al.*, "A Practical Beginner's Guide to Cyclic Voltammetry" *J. Chem. Educ.* 95, 197–206, (2018)

Non-Thermal Protein Structural Change by THz Pulsed Light Irradiation

Kyosuke Makino and Kazuhiko Misawa

Department of Applied Physics, Tokyo University of Agriculture and Technology, 2-24-16 Naka-cho, Koganei, Tokyo, 184-8588, Japan
s229771s@st.go.tuat.ac.jp

Abstract: Terahertz (THz) light that resonates with the vibrational frequency of hydrated water molecules, can alter functional expression of proteins. Previous studies have shown that high-intensity THz light promotes actin fiber formation, but such mechanism is not comprehensively investigated. Here, we aim to clarify this mechanism by irradiating actin solution with THz pulsed light of lower average power and higher electric field intensity to suppress thermal effects. We compare the degree of fiber formation with and without irradiation.

1. Introduction: Water molecules around proteins form a hydration structure that contributes to the stabilization of protein structure and functional expression. In general, terahertz (THz) light that resonates with the vibrational frequency of hydrated water molecules, can alter the functional expression of proteins [1,2]. Previous studies have shown that high-intensity THz light (pulse duration 10 ms, frequency 0.5 THz, maximum amplitude 1.8 V, average power 0.6 mW/cm²) promotes actin fiber formation [3]. They expected that such fiber formation resulted from the reconstruction of water hydration network due to the nonthermal effect of THz excitation for vibrational mode of hydration water. However, this study does not comprehensively clarify whether the promotion of actin fiber is due to the nonthermal effect of intense electric fields or thermal effects originating from the temperature rise by THz light irradiation. In this study, we aim to clarify the existence of non-thermal effects in protein structural change by irradiation with THz pulsed light of lower average power and higher electric field intensity.

2. Methods: The experimental system is shown in Figure 1. We used a THz light pulse with a pulse width of 3-4 ps, a center frequency of 0.7 THz, a peak electric field intensity of approximately 80 V and average power 1.8×10^{-3} mW/cm² generated by the optical rectification effect of a femtosecond laser (center wavelength: 800 nm) using a nonlinear optical crystal (4-N,N-dimethylamino-4-N-methyl-stilbazolium 2,4,6-trimethylbenzenesulfonate: DSTMS). Actin fiber formation is initiated by adding buffer containing divalent cations (Ca²⁺, Mg²⁺) to monomeric actin solutions. The actin is labeled with pyrene, which increases fluorescence (excitation at 365 nm, emission peak at 400 nm) as the fiber formation progresses. Then, we measured fluorescence intensity in 400-500 nm using an optical fiber and a photomultiplier tube (PMT).

3. Results and Discussion: Comparative results (Figure 2) show that the fluorescence intensity was higher for actin irradiated with THz light, which indicates that the THz light pulses inhibit actin fiber re-decomposition, probably due to non-thermal effects. The dependence on the resonant frequency of terahertz light is the key to validate the non-thermal effect. We will change the irradiation condition of THz frequency to clarify the resonant frequency effect.

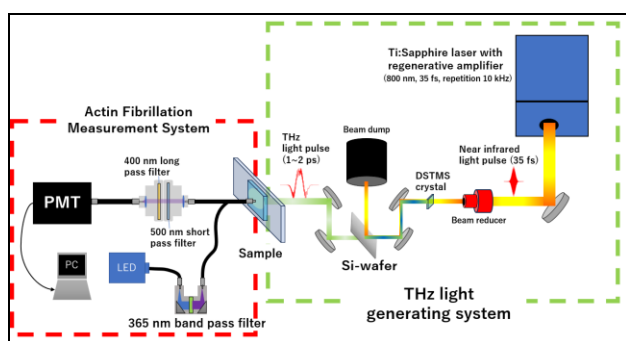


Figure 1: Overview of the experimental system

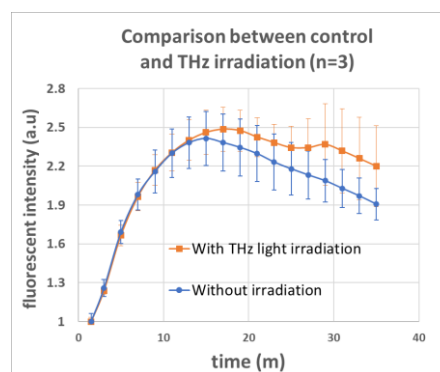


Figure 2: Actin fiber formation with and without THz light irradiation

References

- [1] J. Sugiyama, Y. Tokunaga, M. Hishida, et al., Nonthermal acceleration of protein hydration by sub-terahertz irradiation, *Nat. Commun.* **14**, 2825 (2023).
- [2] I. V. Lundholm, H. Rodilla, W. Y. Wahlgren, et al., Terahertz radiation induces non-thermal structural changes associated with Fröhlich condensation in a protein crystal, *Struct. Dyn.* **1**, (2015).
- [3] S. Yamazaki et al., Actin polymerization is activated by terahertz irradiation, *Sci. Rep.* **8**, 9990 (2018).

Evaluation of the ability of various peptoids to inhibit amyloid beta aggregation

Ogiryama Kei and Kazuhiko Misawa

Tokyo University of Agriculture and Technology, 2-24-16 Naka-cho, Koganei-shi, Tokyo 184-8588

e-mail address: s233864q@st.go.tuat.ac.jp

Abstract: Peptides that inhibit the aggregation of amyloid- β (A β), the causative agent of Alzheimer's disease (AD), have attracted much attention as a treatment for AD. However, peptides have challenges in protease degradation and cell membrane permeability. Peptidomimetics are attracting attention to overcome these challenges. In this study, peptides with A β aggregation inhibitory ability are converted to peptoids, one of the peptidomimetics, and their aggregation inhibitory ability and changes in cell membrane permeability are evaluated. A preliminary experiment showed that A β aggregation without peptoids reaches a steady state in 7 hours.

1. Introduction

Peptides have attracted attention as biopharmaceuticals due to their high biocompatibility, specificity, and low toxicity. Peptide drugs have the potential to be a causative therapy because they can act directly on neurodegenerative diseases caused by abnormal aggregation of proteins and peptides. Alzheimer's disease (AD) is one of the most common neurodegenerative diseases, and although it is the most common form of dementia, there is no fundamental cure for it. For this reason, many studies have been conducted to develop therapeutic agents for AD, including peptides to inhibit the aggregation of the causative agent of Alzheimer's disease (amyloid- β (A β)). However, peptides are subject to protease degradation and have low permeability through cell membranes. Thus, it is important to overcome these disadvantages to use peptides as therapeutic agents. Peptidomimetics have attracted attention as molecules that overcome these disadvantages while retaining the biological activity and function of peptides^[1]. Peptoids are molecules with side chains shifted from α -carbons to nitrogen. This structure makes them resistant to protease degradation and increases their cell membrane permeability, which can improve their biocompatibility. A previous study has shown that peptoids prepared from peptides with A β aggregation inhibition ability could improve the aggregation inhibition ability and blood-brain barrier permeability^[2]. However, it is difficult to conclude that the conversion to peptoids really changed the characteristics, as the previous study compared only one case.

The purpose of this study is to evaluate the usefulness of peptoids as a therapeutic agent for AD by converting some peptides that have already been shown to inhibit A β aggregation into peptoids. We measure how their aggregation inhibition ability and blood-brain barrier permeability are altered. The thioflavin T (ThT) assay is used to evaluate the aggregation inhibition ability. It is known that A β s form the β -sheet structure when aggregated, and ThT can specifically produce fluorescence to the β -sheet structure. This allows us to compare the changes in A β aggregation with and without peptoids. Here we present a preliminary experiment without peptoids and with A β only. The result showed that the fluorescence value of ThT increased with aggregation and reached a steady state after 7 hours.

2. Result and Discussion

A β was adjusted to 100 μ M with DMSO and pure water and incubated at 37°C, shaken at 400 rpm. Fluorescence measurements were then performed using ThT every 30 minutes (up to 8 hours) and 24 hours later. The time variation of the total fluorescence values is shown in Figure 1. The fluorescence value increased with time, indicating that A β aggregation was taking place. The fluorescence value reached the maximum after 7 hours and remained almost unchanged thereafter, indicating that all A β in the solution had been fully aggregated. In the next step, we will measure the aggregation of A β when peptoids are added.

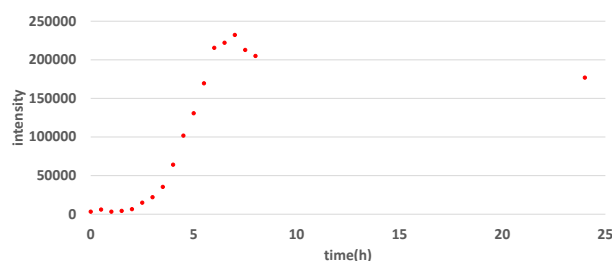


Figure 1 Time variation of ThT fluorescence intensity during A β aggregation

3. References

- [1] Khalily M.P., Soydan M., WILEY Chem Biol Drug Des. Volume 101, Issue 3,772-793 (2022).
- [2] K. Pradhan et al, ACS Chem.Neurosci. **10**,1355-1368 (2019).

Differential Effects of Continuous and Pulsed UV-C Light on Bacterial Inactivation in Platelet Concentrates

Shuri Kozuka, Shundai Yamamoto, and Terumasa Ito

*Department of Biomedical Systems Engineering, Faculty of Engineering, Tokyo University of Agriculture and Technology
s202106z@st.go.tuat.ac.jp*

Abstract: Platelet concentrates (PCs) are prone to bacterial growth due to storage at room temperature. Therefore, an efficient bacterial inactivation technique is desirable. A previous study has shown that pulsed UV-C light inactivates bacteria more effectively than continuous UV-C light under the same irradiation dose. However, the cause of the improved inactivation efficiency has not been elucidated. We show comparative experiments with different UV irradiation conditions to clarify the mechanism of the improved inactivation efficiency.

Blood products are used in transfusion medicine and must be supplied safely to patients. Among blood products, platelet products are particularly difficult to control safety. Platelet concentrates (PCs) are stored at room temperature to maintain hemostatic capacity but are prone to bacterial growth. Transfusion of platelet products contaminated with bacteria can induce sepsis. Therefore, bacterial inactivation is desirable during the production and storage of PCs.

One method for inactivating bacteria in PCs is to combine the addition of photosensitizers with UV-A or UV-B light irradiation, which can achieve a high inactivation effect [1,2]. However, toxic photosensitizers must be removed after irradiation. There is also a concern that the safety of the chemicals cannot be guaranteed. Another alternative method that does not require the addition of chemicals is UV-C light irradiation [3]. This method provides an inactivation effect but does not maintain platelet function such as aggregation capacity. To solve this problem, methods to enhance the inactivation effect by pulsed UV-C irradiation have been proposed [4,5]. Our previous study has shown that pulsed light inactivates bacteria more effectively than continuous light under the same irradiation dose of UV-C [5]. However, the mechanism of the improved inactivation efficiency has not been elucidated.

The aim of this research is to clarify the cause of the higher bacterial inactivation effect of UV-C pulsed light to find effective inactivation conditions, and to develop efficient inactivation techniques. The difference between continuous light irradiation and pulsed light irradiation lies in their instantaneous peak power and pulse energy per irradiation. Which of these enhanced the inactivation effect was not known in the previous study. To clarify this, two experiments will be conducted. In the first experiment, we will compare the bacterial inactivation under irradiation conditions in which only the pulse width is changed under the same repetition frequency of 10 kHz, which will show whether the high peak power of the pulsed light contributes the inactivation enhancement. In the second experiment, we will compare the bacterial inactivation under irradiation conditions with the same pulse width but with different repetition frequency of the light source. The result will show the pulse energy dependence of the inactivation efficiency.

Currently, we are revisiting our previous experiment on comparing the bacterial inactivation effects with a continuous wave LED and a femtosecond pulsed laser. We have confirmed that the effectiveness of the pulsed UV-C inactivation is reproducible. This presentation will describe two methods to test which parameters of pulsed light irradiation enhance the inactivation effect.

References

- [1] J. Irscha and L. Linb, "Pathogen Inactivation of Platelet and Plasma Blood Components for Transfusion Using the INTERCEPT Blood System™," *Transfus Med. Hemother.* **38**, 19–31 (2011).
- [2] P. H. Ruane, et al., "Photochemical inactivation of selected viruses and bacteria in platelet concentrates using riboflavin and light," *Transfusion* **44**, 1537-2995 (2004).
- [3] A. Seltsam and T. H. Müller, "UVC Irradiation for Pathogen Reduction of Platelet Concentrates and Plasma," *Transfus. Med. Hemother.* **38**, 43–54 (2011).
- [4] H. Abe, et al. "Pulsed xenon flash treatment inactivates bacteria in apheresis platelet concentrates while preserving in vitro quality and functionality," *Transfusion* **57**, 989-996 (2017).
- [5] M. Saiga, et al., "Bacterial Inactivation in Platelet Concentrates Using Ultrashort Pulsed Laser," *Proc. SPIE*, 119210J (2021).

Real-Time Monitoring of Aspirin Metabolism Using Raman Microscopy

Ryo Fujisawa and Terumasa Ito

Department of Biomedical engineering Tokyo University of Agriculture and Technology, 2-24-16 Naka-cho, Koganei, Tokyo, Japan
s207975s@st.go.tuat.ac.jp

Abstract: Monitoring of aspirin and its metabolite concentrations would be desirable to prevent poisoning effect while adjusting the dose at the optimum concentration. In this study, we show that Raman spectroscopy can be used to perform real-time monitoring of aspirin metabolism. A preliminary spectral measurement of aspirin and its metabolites using confocal Raman microscopy show that each chemical has different peaks in the Raman spectrum.

1. Introduction

In living organisms, drugs are processed through the processes of absorption, distribution, metabolism and excretion, which are considered essential for the pharmacological activity and efficacy of administered chemicals. Among them, metabolism is particularly important because many drugs show efficacy or toxicity depending on their metabolism. As an example, aspirin, which is an antipyretic, analgesic, and anti-inflammatory drug, is mainly metabolized in the liver to salicylic acid. However, excessive aspirin intake can lead to salicylic acid poisoning, which can lead to liver and kidney damage. In fact, in the treatment of rheumatic fever, the concentration of salicylic acid in the plasma is close to the intoxication range [1]. To prevent salicylic acid poisoning while adjusting the aspirin dose at the optimum concentration, simultaneous monitoring of aspirin and salicylic acid concentrations would be desirable.

One conventional analytical method to simultaneously detect aspirin and salicylic acid is liquid chromatography-mass spectrometry (LC/MS) [2]. However, LC/MS requires complex and laborious sample processing from sample collection to measurement. Another promising candidate is Raman spectroscopy, which is a label-free laser spectroscopy to analyze the molecular structure of chemicals by examining frequency-shift dependence of the scattered light (Raman spectrum). Raman spectroscopy does not require complex processing of the sample and allowing rapid detection of drugs in the body. Therefore, it can be used to determine real-time aspirin and salicylic acid concentrations for optimizing individual patient dosing.

The aim of this study is to monitor aspirin metabolism in real-time using Raman microscopy. As a preliminary experiment, Raman spectra of aspirin, and its metabolites (salicylic acid and acetic acid) were measured using confocal Raman microscopy. The results show that the Raman spectra of aspirin, salicylic acid and acetic acid have different peaks.

2. Methods and results

Aqueous solutions of aspirin, salicylic acid, and acetic acid were prepared (aspirin 6.5 mM, salicylic acid saturation concentration (< 68 mM), acetic acid 1.5mM) and Raman spectra were measured by confocal Raman microscopy. The results are shown in Figure 1.

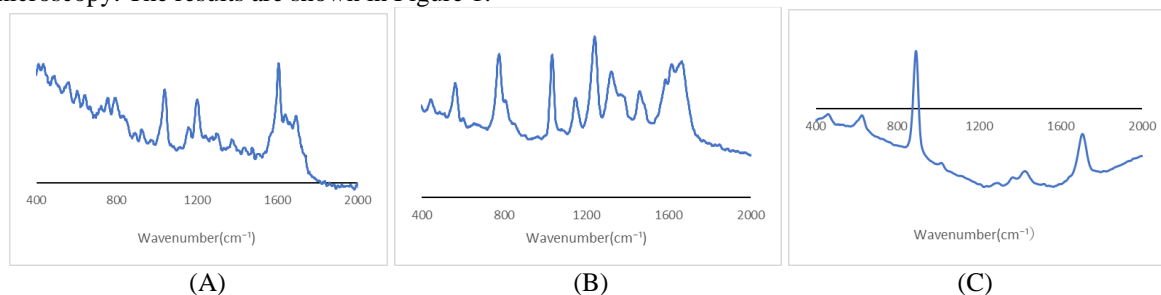


Fig. 1. Measured Raman spectra: (A) aspirin, (B) salicylic acid, and (C) acetic acid

3. Discussion

We found that each chemical exhibits a unique, distinct peak: aspirin at 1607 cm^{-1} , salicylic acid at 564 cm^{-1} , and acetic acid at 890 cm^{-1} . Since these peaks are not found in other substances, monitoring the changes in the intensity of these peaks will allow us to observe aspirin metabolism. As a next step, we will conduct an experiment to monitor the aspirin and the metabolites while aspirin is hydrolyzed with esterase.

References

- [1] Bayer Yakuhiin K.K., Drug Interview Form “Bayaspirin tablets 100 mg” (2019) (in Japanese) https://pharma-navi.bayer.jp/sites/g/files/vrxlpx9646/files/2022-05/BAS_IVF_202205120.pdf
- [2] D. Sirok et al., “Robust and sensitive LC/MS-MS method for simultaneous detection of acetylsalicylic acid and salicylic acid in human plasma,” *Microchemical Journal* **136**, 200-208 (2018)

Analysis of Cellular Transport of Odor Molecules Using Coherent Raman Scattering Microscopy

Noa Saito and Terumasa Ito

Department of Biomedical Engineering, Tokyo University of Agriculture and Technology, 2-24-16 Naka-cho, Koganei, Tokyo, Japan
s209904u@st.go.tuat.ac.jp

Abstract: Despite the advances in the understanding of olfactory receptors, the detailed transport dynamics of odor molecules themselves has not been fully understood. Using coherent Raman microscopy, a high-speed label-free chemical imaging method, we investigate whether the odorants that bind to receptors are taken up into the cells.

1. Introduction

Advances in olfactory research would help develop odor sensors that enable early diagnosis and prevention of diseases. When an odor molecule enters the nasal cavity, it binds to olfactory receptors and electrical signals are sent out to recognize the odor. Various odors can be identified by the combined binding of receptors consisting of about 400 different receptor types. The research focus in this field has been to explore the interactions between olfactory receptors and odor molecules, where luciferase chemiluminescence reporters are often used to examine the odor-receptor binding strength. Despite the advances in the understanding of olfactory receptors, the detailed transport dynamics of odor molecules themselves has not been fully understood. There are two possible membrane transport pathways: namely, passive diffusion and receptor-mediated transport. Passive diffusion is considered as the major pathway of odor molecules due to their small size (molecular weight of approximately 200) and lipophilicity. In addition to this, receptor-mediated transport can be considered as the second transport mechanism. However, there is no evident report that the olfactory receptor actively pumps odorants into the cell. The challenge in such research lies in the difficulty in the direct observation of odor molecules. Due to the small size of odorants, one cannot use labelling such as fluorescence tags since it may alter the transport kinetics and physiological functions, which makes it difficult to monitor the local concentration of the odor molecules in live cells.

In this study, we analyze the cellular transport of odor molecules using Raman microscopy. Raman microscopy is a label-free chemical imaging method that can be used for observing small molecules [1]. Conventional Raman microscopy suffers from low sensitivity and does not support real-time small-molecule detection. However, this issue can be overcome by using coherent Raman scattering microscopy [2], which can amplify the signal intensity via pulsed excitation by up to several orders of magnitude. With this technique, we will clarify whether the odorants that bind to receptors are taken up into the cells.

2. Methods

To investigate the receptor-mediated transport, cells expressing an olfactory receptor that binds to the target odorant molecule, and cells expressing another different olfactory receptor with no binding to the odorant are prepared. We use our developed coherent Raman microscope that is designed to detect small molecules with enhanced signal contrast [2]. If the receptor pumps the odorant into the cells, we should be able to observe an increased concentration inside the cell, in addition to the passively transported odorants. The measurable intracellular concentration of the odorant by coherent Raman microscopy is determined by the signal-to-background ratio, i.e., the ratio of the spectral intensity of the odor molecules to the background spectral intensity of the cell. Therefore, we first measured the background Raman spectrum of the cell.

3. Results and Discussion

Figure 1 shows the background spectrum of the cultured cells measured with the coherent Raman microscope. The spectrum shows a peak around 1000 cm^{-1} (phenylalanine in proteins) with a relatively large signal. To optimize the measurement accuracy, an odorant that has a clear peak other than this wavenumber area should be selected. Based on this data, we will conduct a screening spectral measurement to select the best model odorant.

[1] Y. Fukutani et al., "Vapor detection and discrimination with a panel of odorant receptors," *Nature Communications* **9**, 4556 (2018).

[2] T. Ito et al., "Spectral focusing with asymmetric pulses for high-contrast pump-probe stimulated Raman scattering microscopy" *APL Photonics* **3**, 092405 (2018).

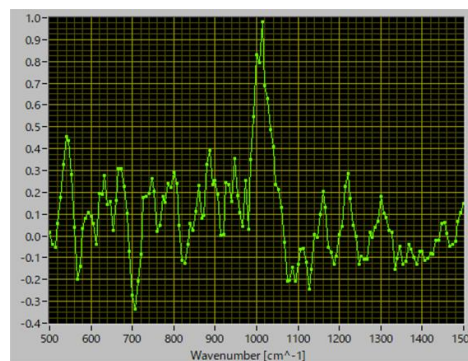


Fig. 1. Raman spectrum of the cells measured by the coherent Raman microscope.

Improvement of kinetic energy conversion via laser induced bubble by pulse shaping

Yuki Uchiyama¹, Satoshi Honma¹, Hironori Ito¹

¹University of Yamanashi, 4-4-37, Takeda, Kofu, Yamanashi, 400-8510, Japan
E-mail: hito@yamanashi.ac.jp

Abstract: When a laser beam is focused on a liquid, bubbles are known to be generated and liquid motion occurs. This technology is expected to be applied to medical analysis technology and cooling technology for electronic components. The problem with this technology is the optical-kinetic energy conversion efficiency. In this study, we demonstrate the superiority of multiphoton excitation by comparing the growth rate of bubbles generated by a femtosecond pulsed laser and a continuous wave laser of the same energy.

1. Introduction

When a laser beam is focused on a small area in a liquid, an extremely high thermal gradient is generated, which induces liquid motion such as expansion and contraction motion [1], and Marangoni convection [2]. This technology is expected to be applied to medical analysis technology, liquid jet scalpels for surgery, and cooling technology for electronic components. Energy not converted to kinetic energy becomes heat, damaging the sample and reducing energy conversion efficiency. Therefore, it is necessary to increase the efficiency of optical-kinetic energy conversion. In this study, we focused on multiphoton excitation induced by femtosecond pulse lasers (fs laser). The rapid thermal gradient due to multiphoton excitation is expected to significantly improve the kinetic energy conversion efficiency. The growth rates of bubbles generated by fs laser and continuous-wave (CW) laser at the same energy were compared to demonstrate the improvement in optical-kinetic energy conversion efficiency by multiphoton excitation.

2. Experimental Methods

The optical system shown in Fig. 1 is designed and constructed to generate bubbles in a liquid by a laser and to observe them. A CW laser with a wavelength of 800 nm and a fs laser with a repetition rate of 76 MHz, a center wavelength of 800 nm, and a pulse width of 15 fs were used as the light sources for bubble generation. These lasers were focused onto a dye precipitate in acetone solution containing methyl elongate using an objective lens to generate bubbles. A bandpass filter transmitting light between 400 nm and 600 nm was used to prevent scattering of the laser beam. A CMOS camera was used for observation.

3. Result

Fig. 2 shows the bubble generation during (a) continuous CW laser irradiation and (b) continuous fs laser irradiation at 200 mW. In the case of fs laser irradiation, emission from two-photon excitation that passed through the filter can be confirmed near the focal point. Fig 3 shows the laser power dependence of the bubble growth rate under CW and fs laser irradiation. At 220 mW and 240 mW, the growth rate of bubbles increases rapidly when irradiated by the fs laser. This indicates that the fs laser irradiation generates bubbles with high efficiency via two-photon excitation.

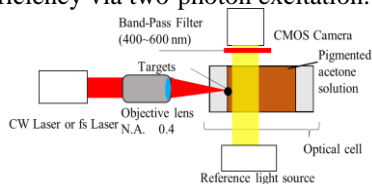


Fig. 1 Optical setup for laser focusing and observation

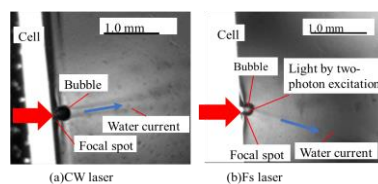


Fig. 2 CMOS images of bubble generation by (a) CW laser, (b) fs laser

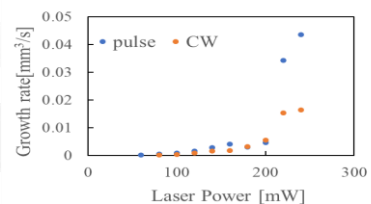


Fig. 3 Laser power dependence of bubble growth rates

4. Conclusion

In this study, the efficiency of bubble generation in single-photon excitation and two-photon excitation was compared by comparing the bubble generation rates in CW and fs lasers. As a result, it was found that bubbles were generated more efficiently with two-photon excitation.

5. References

- [1] Y. Mizushima et al., Appl. Phys. Lett. 107 114102 (2015).
- [2] K. Namura et al., Scientific Reports 9 4770 (2019).

Control of lattice vibrations by carrier-envelope phase modulation of terahertz pulses

Ryuta Watanabe¹, Satoshi Honma¹ and Hironori Ito¹

¹University of Yamanashi, 4-4-37, Takeda, Kofu, Yamanashi, 400-8510, Japan
E-mail: hito@yamanashi.ac.jp

Abstract: This presentation suggests a fast control of lattice vibrations by modulating the carrier envelope phase of double terahertz pulses using a modified Michelson interferometer. A resonant EO sampling technique is also proposed to dynamically observe the instantaneous stopping of oscillating lattice vibrations.

1. Introduction

Currently, methods to excite lattice vibrations by electromagnetic pulses at terahertz frequencies (THz pulse) are attracting attention. Recently, it has been reported that lattice vibrations can induce physical properties such as superconductivity [1] and magnetic fields, and there is a possibility that these properties can be controlled at high speed by controlling lattice vibrations with THz pulses.

In previous study, a single THz pulse is used to induce lattice vibrations [2] as shown in Fig. 1(a). In this study, a second THz pulse is introduced as shown in Fig. 1(b). Furthermore, by manipulating the carrier envelope phase of the second THz pulse, we propose a method to instantly stop the lattice vibration and control it at high speed. The realization of this method is expected to speed up the control of physical properties associated with lattice vibrations. In this study, the generation of double terahertz pulses will be aimed for, lattice vibration will be induced, oscillation will be controlled and halted, and the oscillation will be observed.

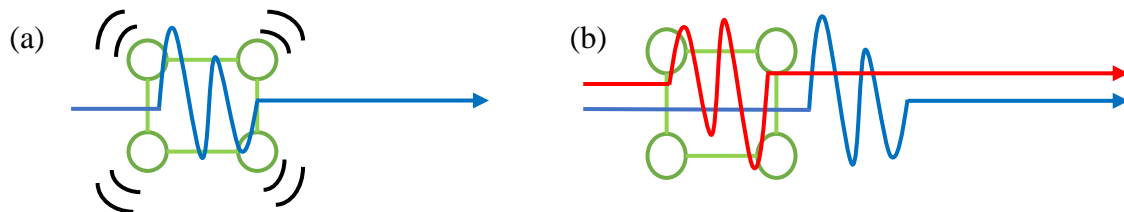


Fig. 1 Schematic diagram of controlling lattice vibration with THz pulse. (a) For single pulse, a lattice vibration is generated. (b) Lattice vibration stops instantly at the second THz pulse with adjusted carrier-envelope phase.

2. Resonant EO sampling for observation of lattice vibration

An observation method is proposed for lattice vibrations controlled at high speed by two terahertz pulses, by EO sampling resonant to the vibrational mode. EO sampling is usually used to measure the instantaneous electric field of THz pulse. Incident of the THz pulse to be observed into an electro-optical crystal distorts the lattice and causes birefringence due to the piezoelectric effect. This anisotropy of the refractive index can be detected as a change in the polarization of the simultaneously injected probe light fs pulse to measure the instantaneous electric field of THz pulse.

The temporal variation of the THz pulse is obtained by shifting the delay time of the probe light. In the case of intrinsic vibrations of the electro-optical crystal within the bandwidth of the incident THz pulse, the lattice vibrations themselves can be observed, although the electric field intensity will not be measured correctly. The suggestion is to use quartz crystals as electro-optical crystals for EO sampling. The terahertz pulses used in this experiment have a centre frequency of about 0.1-10 THz, which resonates with the vibrational mode of the 3.1 THz infrared activity of quartz.

The peak of the vibrational mode is sharp and has a lifetime of about 10 ps. The electro-optical coefficient of quartz is small and not suitable for intrinsic EO sampling, but is increased by the intrinsic vibration and can be detected. The first terahertz pulse will be used to induce vibrational mode in the quartz crystal, and the carrier envelope phase of the second pulse will be adjusted to stop the vibrational mode.

3. References

- [1] T. F. Nova, A. Cartella, A. Cantaluppi, M. Forst, D. Bossini, R. V. Mikhaylovskiy, A. V. Kimel, R. Merlin, and A. Cavalleri, "An effective magnetic field from optically driven phonons," *Nat. Phys.* 13, 132–136 (2017)
- [2] C. Vicario, A. Trisorio, S. Allenspach, C. Ruegg, and F. Giorgianni, "Narrow-band and tunable intense terahertz pulses for mode-selective coherent phonon excitation" *Appl. Phys. Lett.* 117, 101101 (2020)

SQAM signal retrieval for holographic memory using a spatial partial filter based on IFTA

Akihiro Yamashita¹, Hironori Ito¹, Satoshi Honma¹

¹University of Yamanashi, 4-4-37, Takeda, Kofu, Yamanashi, 400-8510, Japan

E-mail: shonma@yamanashi.ac.jp

Abstract: We propose a retrieval method based on IFTA to detect SQAM signals with simple optics, by blocking a part of the reconstructed beam with a spatial partial filter. The numerical analysis shows our technique can retrieve SQAM data with less embedded data.

1. Introduction

The recording scheme of spatial quadrature amplitude modulation (SQAM) signals improve the density of holographic data storages (HDS) [1]. One method based on Iterative Fourier Transform Algorithm (IFTA), which retrieves the phase from the intensity distribution in the Fourier plane of the reconstructed beam without optical interferometers was proposed [2]. However, to achieve sufficient accuracy, a certain amount of known data (embedded data) must be embedded in the recorded data. This reduces the effective storage capacity.

In this paper, we propose a novel IFTA method to reduce the amount of embedded data by blocking a part of the reconstructed beam with a spatial partial filter. It reduces storage loss due to embedded data.

2. IFTA method using a spatial partial filter

The reading process is shown in Fig. 1. The SQAM signal is reconstructed from the HDS. After passing through the lens, the beam enters the spatial partial filter in the object domain. The light near the boundary of each data area is blocked by the filter. On the other hand, the light in the embedded data area is transmitted without being blocked. After the beam passes through the lens again, the Fourier intensity I_F is captured by a CMOS sensor.

The retrieval process of complex amplitude based on IFTA is described in Fig. 2. g_k indicates an estimate SQAM signal data. Then, the value of g_k is replaced with embedded data. After the substitution, obtained distribution is redefined by g'_k . Executing the Fourier transform on g'_k , we obtain G_k on the Fourier domain. After replacing $|A_{F,k}|$ with the square root of the Fourier intensity I_F , the distribution is redefined by G'_k . By performing the inverse Fourier transform on G'_k , we obtain the g_{k+1} , which is the new estimate for the iteration.

3. Numerical analysis of SQAM signals retrieval

We evaluated the retrieval accuracy for 10 pages of SQAM signal composed of 64×64 symbols, with 4-level phase and 2-level amplitude values. The area of a symbol was defined as $L \times L$, and the transmission area of the spatial partial filter was $(L/2) \times (L/2)$.

The number of iterations until the symbol error rate (SER) reaches 0 % under different embedded rate is plotted in Fig. 3. As the embedded rate decreased, the iterations required for retrieval increased. Our method can retrieve the data with 10 iterations and 20 % embedded rate. However, the conventional method requires 50 % embedded rate to retrieve data within 10 iterations.

4. Conclusions

We proposed a retrieval method for the SQAM signal using the spatial partial filter and IFTA. Our method can retrieve SQAM data with less embedded data, comparing with the conventional method.

5. References

- [1] S. Honma and H. Funakoshi, "Reproduction of SQAM signal for holographic memory and Estimation of recording density", IEICE technical report, 2020, vol. 119, no. 421, pp. 283-288.
- [2] C. Yu, S. Wang, R. Chen, J. Hao, Q. Zheng, J. Wang, X. Qiu, K. Wang, D. Lin, Y. Yang, H. Li, X. Lin, and X. Tan, "Improved phase retrieval in holographic data storage based on a designed iterative embedded data", Front. Optoelectron 14, 2021, pp. 529-539.

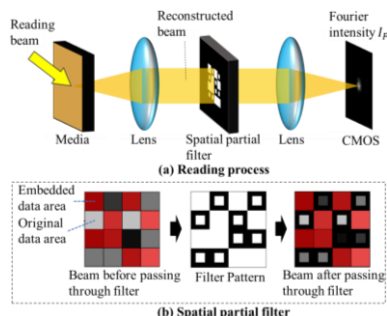


Fig. 1 Reading process

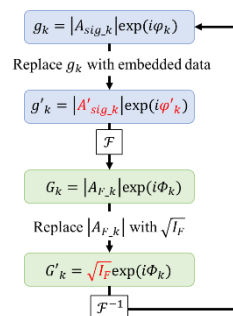


Fig. 2 Retrieval process of IFTA

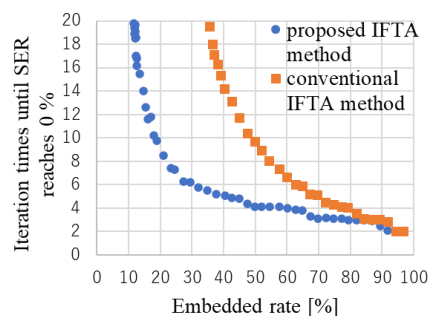


Fig. 3 Numerical analysis result

Decoding method with simultaneous reconstruction of SQAM signals for holographic data storage

Yunosuke Shimizu, Hironori Ito, Satoshi Honma

University of Yamanashi, 4-4-37, Takeda, Kofu, Yamanashi, 400-8510, Japan
E-mail: i20ee025@yamanashi.ac.jp

Abstract: We propose a simple optical system to decode complex amplitude of the reconstructed SQAM signal by simultaneously reproducing multiple SQAM signal beams and detecting the interference fringe of the beams. We estimate the quality of the detected complex amplitude of the signal by the numerical analysis.

1. Introduction

Many researchers have investigated recording schemes of spatial quadrature amplitude modulated (SQAM) signal to increase the capacity of holographic data storage (HDS). Optical interferometers are in general used to measure the phase of the reconstructed signal light, which complicates the optical system.

In this report, we propose a new decoding method of the SQAM signals, in which multiple SQAM signal are simultaneously reproduced from HDS and the interference fringe pattern are detected by camera, without external optical interferometer. The phase distribution of the signals is measured by analyzing the fringe pattern. In the following, we evaluate the estimation accuracy of the reproduced distributions.

2. Recording process of SQAM signal and decoding process by simultaneous reconstruction

Figure 1 shows a recording process of the SQAM signals. The signal Fourier transformed by a lens and the reference light are irradiated on the holographic disc, and the hologram is recorded. And then, the series of holograms are recorded by the same process, rotating the disc.

Figure 2 shows a schematic diagram of the simultaneous reconstruction of two SQAM signals and the decoding the complex amplitude of the signal. The two holograms are simultaneously readout and then the interference pattern of the reproduced signal beams are detected by the camera. Implementing Fourier fringe analysis to the pattern, we obtain the distribution corresponding to $C_2 C_1^*$, where $C_i(x, y)$ is the complex amplitude value of each SQAM signal recorded in holographic memory and the subscript $i = 1, 2$ are the label number of the holograms[1]. Here, if the distribution of C_1 is known in advance, C_2 can be calculated by dividing $C_2 C_1^*$ by C_1^* .

3. Evaluation of estimation accuracy

We assume the SQAM signal, composed of 32×32 pixels, whose amplitude and phase are modulated to two levels of 0.5, 1 and four levels of $0, \pi/2, \pi, 3\pi/2$, respectively. The SQAM signal corresponding to C_1 and C_2 are reproduced from the adjacent holograms, and then the C_2 is decoded by our technique with C_1 . The calculation result of it is shown in Fig. 3. Although distortion occurs near the boundary of each pixel, it can be confirmed that the complex amplitude value is estimated with relatively high accuracy.

The estimated signal can be used to decode adjacent neighboring holograms. As a result, all holograms in the holographic memory can be sequentially decoded while the disk is rotated and reproduced.

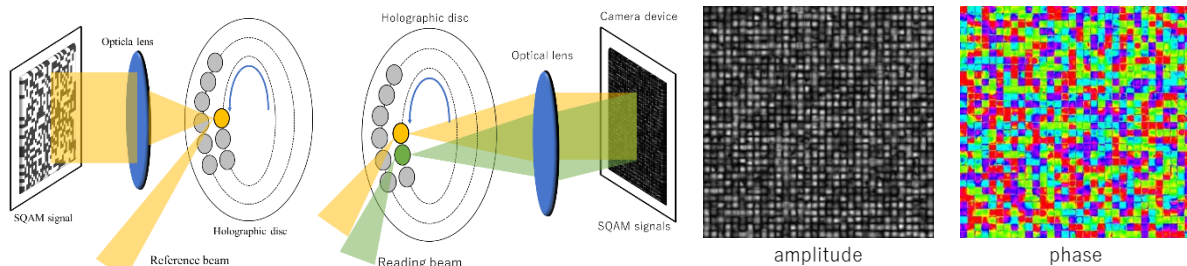


Fig.1. Recording process

Fig.2. Reading process

Fig.3 Decoded SQAM signals using known C_1

4. Conclusions

We designed the simple optical system to detect the phase distribution of the SQAM signal without an optical interferometer. It was shown that if the distribution of one SQAM signal is known, the other SQAM signal distribution can be decoded with relative

ely good accuracy from the interference pattern between the signals.

5. References

[1] M. Takeda, H. Ina, and S. Kobayashi, "Fourier-transform method of fringe-pattern analysis for computer-based topography and interferometry," J. Opt. Soc. Am., 72, pp.156-160 (1982).

Energy Transfer Between Quantum Dots and Monolayer MoS₂ Studied by Ultrafast optical Pump-Probe Spectroscopy

Yi-Hung Lin¹, Yu-Chan Tai¹, Jhen-Dong Lin¹, Bo-Jun Lai¹⁺, Rwei-Jhe Tu¹, Shao-Yu Chen^{2,3}, Chun-Liang Lin¹, Shun-Jen Cheng¹, Chih-Wei Luo¹

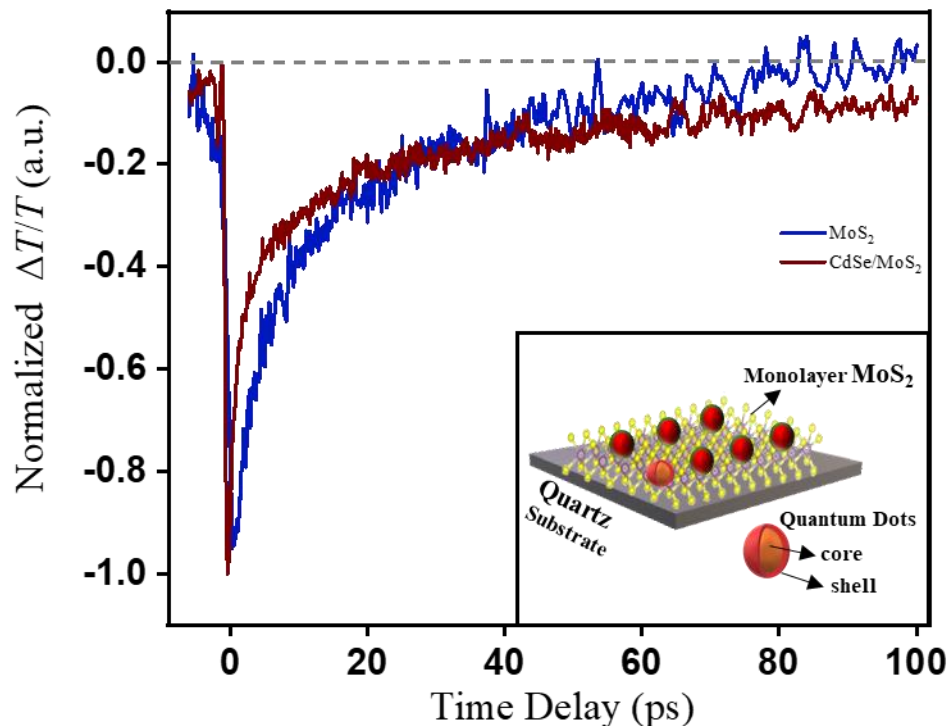
¹Department of Electrophysics, National Yang Ming Chiao Tung University, Hsinchu, 30010, Taiwan

²Center of Atomic Initiative for New Materials, National Taiwan University, Taipei, 10617, Taiwan

³Center for Condensed Mater Science, National Taiwan University, Taipei, 10617, Taiwan

Email: zach.sc11@nycu.edu.tw

Abstract: We observed the nonradiative energy transfer (NRET) in the hybrid structure of semiconducting quantum dots (QDs) spin-coated on a monolayer (ML) molybdenum disulfide (MoS₂). This study investigated the ultrafast dynamics of excitons in the ML MoS₂ with and without the QDs using optical pump-probe spectroscopy (TRS). From photoexciting the heterostructure of QDs/MoS₂, we obtained a faster relaxation and a longer lifetime in the transient transmission spectra. By inspecting the energy levels of QDs and ML MoS₂, we address the dipole-dipole coupling between QDs and ML MoS₂ as the observation of NRET that appeared in the photoexcited heterostructure of QDs/MoS₂.



Normalized transient transmission spectra from heterostructure of QDs (CdSe) / MoS₂. Inset: heterostructure of QDs/MoS₂

Ultrafast dynamics of CrMnFeCoNiO_x thin film by pump-probe spectroscopy

Hsing-Yu Yeh¹, Chien-Ming Chen^{1*}, Wen-Yen Tzeng², Wei-En Ke³,
Yu-Chan Tai², Ying-Hao Chu³, Chih-Wei Luo^{1,2}

¹Department of Physics, National Yang Ming Chiao Tung University, Hsinchu, Taiwan

²Department of Electrophysics, National Yang Ming Chiao Tung University, Hsinchu, Taiwan

³Department of Materials Science and Engineering, National Tsing Hua University, Hsinchu, Taiwan

* Presenter: Chien-Ming Chen, Email: chienming.sc11@nycu.edu.tw

Abstract:

We present a temperature-dependent two-color optical pump-probe spectroscopy study of the high-entropy alloy oxide, CrMnFeCoNiO_x films. Transient reflectivity changes reveal damped oscillations spanning 300 K to 20 K, with extracted natural frequencies using fast Fourier transform. Damped sine function modeling characterizes oscillation lifetimes. Notably, a speculated phase transition around 160 K is indicated by consistent lifetimes. Our report sheds light on oscillation generation and data analysis through pump-probe spectroscopy of CrMnFeCoNiO_x films.

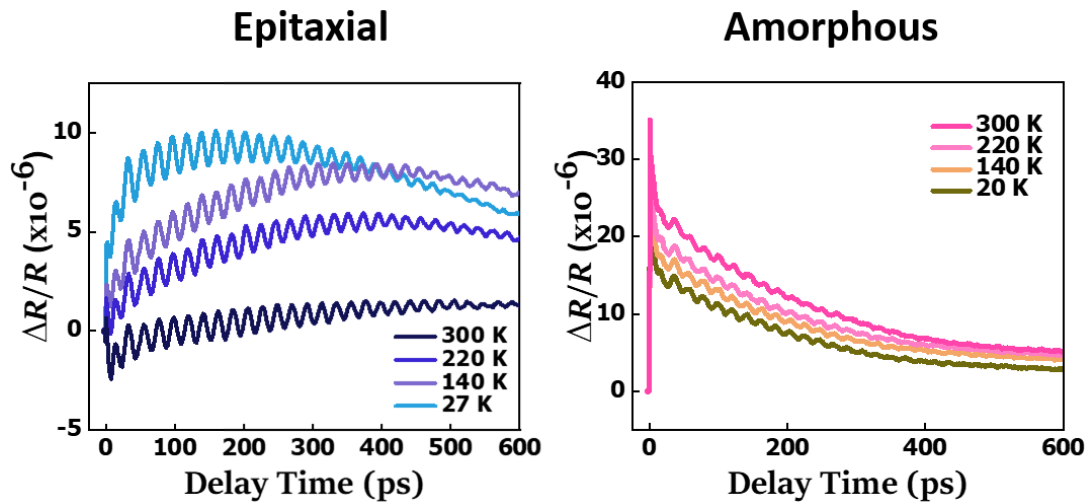


Figure . Using pump probe spectroscopy experiment on (a) Epitaxial (b) Amorphous type thin film in the range of delay time from 0 to 600 ps.

Encoding information into Terahertz pulses via spectrally modulated ultrafast optical pulses

Ching-Wen Wang¹, Nai-Hao Chiang², Yu-Chan Tai², Wei-Hong Huang², Chih-Wei Luo²

¹Department of Physics, National Yang Ming Chiao Tung University, Hsinchu 300, Taiwan.

²Department of Electrophysics, National Yang Ming Chiao Tung University, Hsinchu 300, Taiwan.

c311658011.sc11@nycu.edu.tw; cwluoep@nycu.edu.tw

Abstract: We tried to achieve Terahertz communication through photoconductive antenna (PCA) working at 800-nm ultrafast optical pulses. Encoding a set of bit-wise information into the waveform of single THz-pulse, which was generated by a PCA. The bit-wise information was encoded via a spatial light modulator (SLM) in frequency domain before the photoexcitation of the PCA. We utilized a grating to split the optical pulses to frequency domain, and employed a SLM to modulate the spectral intensity of optics pulses. The spectral frequency of pulses can be determined to pass or to be blocked by the designed pattern of the SLM. The selectively modulated pulses will stimulate the PCA and generate corresponding THz waveforms. Our simulation demonstrates that THz waveforms exhibit varying responses under different spectrally modulated injected pulses.

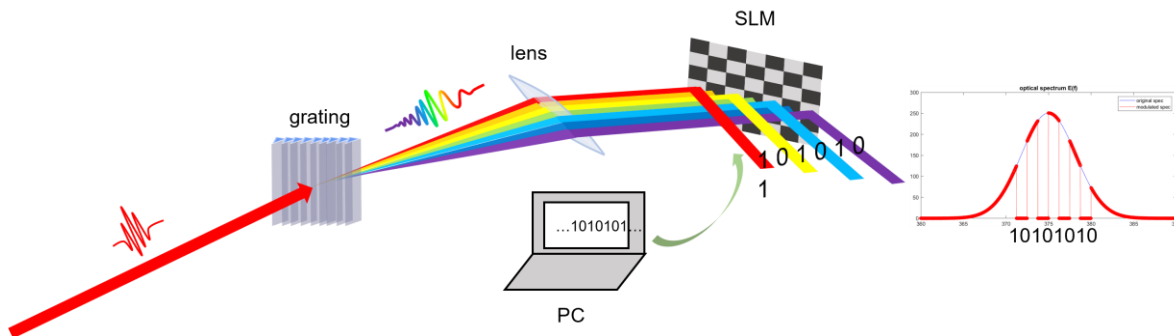


Figure 1. The schematic of spectrally modulated ultrafast optics pulsed before the photoexcitation of the PCA.

Using Mid-Infrared Pulses via Four-Wave Difference Frequency Generation to Observe Catalytic Materials

Chun-Ying Lin¹, Chien-Ming Chao², Wei-Hong Huang¹, Chih-Wei Luo¹, Yu-Jung Chen², Meng-Fan Luo²

¹Department of Electrophysics, National Yang Ming Chiao Tung University, Hsinchu, 300093 Taiwan

²Department of Physics, National Central University, Taoyuan City 320317, Taiwan

Author e-mail address: chunying.sc11@nycu.edu.tw

Abstract: We will focus two-color filamentation to generate mid-infrared (MIR) pulses via four-wave difference frequency generation [1] and make the MIR pulses as probe beam for measurement. To minimize dispersion of MIR pulses, we will decrease using transmissive optical components in our system. For the detection part, we can use a reference beam to have collinear focus with our MIR light source for up-converting photon energy from MIR region to visible region through gaseous medium [2]. This up-conversional method is more convenient and quicker to measure MIR spectrum based on the detected up-conversional visible spectrum. To monitor reactions within MIR region and check mass spectroscopies simultaneously, a near-ambient pressure (NAP) reaction cell was required, and that was installed inside the ultrahigh vacuum (UHV) chamber. The NAP and UHV chamber were designed by our team member of NCU. This UHV chamber can be used to observe the dynamics of catalytic reactions which occurred on the surface of sample [3]. In our plan, the sample was Rh nanoparticles which were grown on NiAl substrate with a AlO₃ coating. We will expose methanol on the surface of sample to have decomposition reaction. The overall configuration was shown in Figure 1.

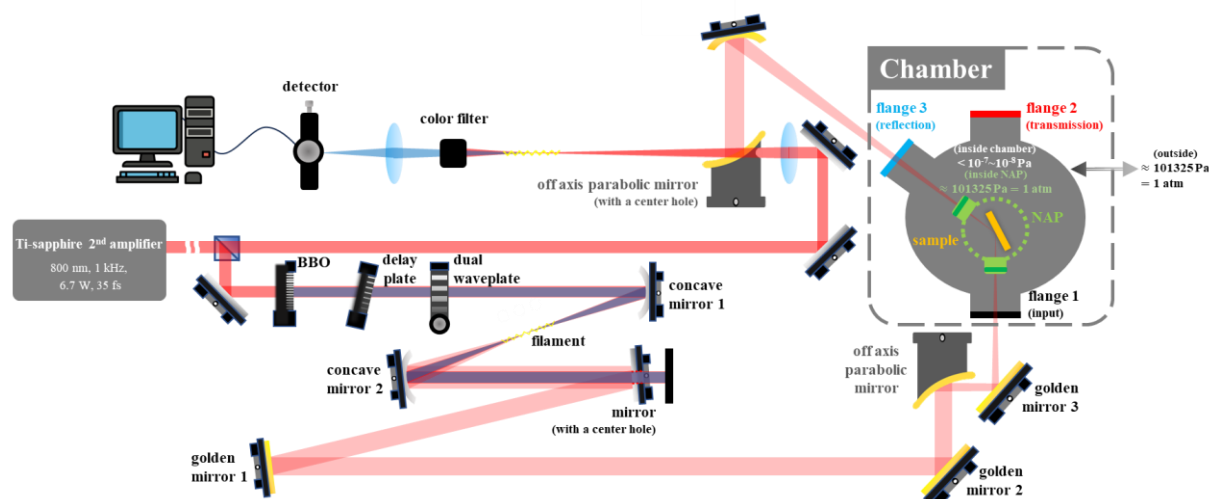


Figure 1. The setup of the MIR pulses generation coupling with UHV chamber system.

References

- [1] Fuji, Takao, and Toshinori Suzuki. "Generation of sub-two-cycle mid-infrared pulses by four-wave mixing through filamentation in air." *Optics letters* 32.22, 3330-3332. (2007)
- [2] Y. Nomura, Y.-T. Wang, T. Kozai, H. Shirai, A. Yabushita, C.-W. Luo, S. Nakanishi, and T. Fuji, "Single-shot detection of mid-infrared spectra by chirped-pulse upconversion with four-wave difference frequency generation in gases," *Opt. Express* 21, 18249-18254 (2013)
- [3] Yunshu Du, Ling Li, Xuan Wang, and Hengshan Qiu, "A Newly Designed Infrared Reflection Absorption Spectroscopy System for In Situ Characterization from Ultrahigh Vacuum to Ambient Pressure," *Appl. Spectrosc.* 72, 122-128 (2018)

Study of Ultrafast Dynamics in Tb_2Te_5 single crystal Using Time-Resolved Spectroscopy

Hsing-Yu Yeh^{1*}, Wen-Yen Tzeng², Nguyen, Nhat-Quyen², Yu-Chan Tai², Chih-Wei Luo^{1,2}

¹Department of Physics, National Yang Ming Chiao Tung University, Hsinchu, Taiwan

²Department of Electrophysics, National Yang Ming Chiao Tung University, Hsinchu, Taiwan

Presenter: Hsing-Yu Yeh, Email: juststartyo@gmail.com

Abstract:

Layered rare earth (R) tellurides layered single crystal RTe_n ($n=2, 2.5, 3$) are considered to be charge density wave (CDW) materials. To gain a better understanding of the ultrafast dynamics of Tb_2Te_5 and determine whether it exhibits CDW behavior, we employed dual-color pump-probe time-resolved spectroscopy at various temperatures, as well as low-temperature X-ray diffraction. In the temperature range of 8 K to 100 K, the transient reflectivity changes ($\Delta R/R$) exhibit a 3.77 THz oscillation mode, and there are distinct trends in the variations of the b-axis length around the temperature of 120 K in the low-temperature X-ray diffraction results. By comparing these findings to CDW-like properties observed in other CDW materials, we conclude that Tb_2Te_5 can be classified as a CDW material, with an estimated CDW phase transition temperature (T_{CDW}) falling in the range of 100-120 K.

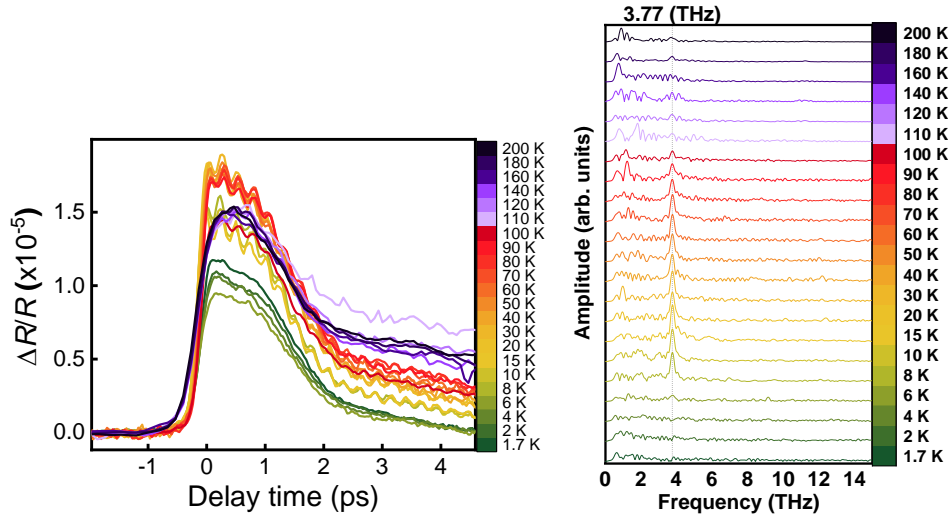


Figure. 1. (a) Pump-probe spectroscopy result in Tb_2Te_5 (b) FFT result in temperature of 1.7 K to 200 K

Ultrafast Carrier Dynamics of the Grain Boundaries in LSMO Homostructure by Spatial Resolved Ultrafast Pump-Probe Spectroscopy

Jia-Yuan Sun^{1*}, Wen-Yen Tzeng¹, Yu-Chan Tai¹, Jan-Chi Yang², Chih-Wei Luo¹

¹Department of Electrophysics, National Yang Ming Chiao Tung University, Hsinchu, Taiwan

²Department of Physics, National Cheng Kung University, Tainan, Taiwan

* Presenter : Jia-Yuan Sun, email: scu1027@gmail.com

Abstract: Perovskite manganites are known as functional materials showing colossal magnetoresistance (CMR) and one of perovskite-LaSr_{1-x}Mn_xO₃ (LSMO) is kind of classic half-metallic oxide that exhibits large spin polarization and CMR effect. Recent research shows that an unconventional butterfly-shaped hysteresis magnetoresistance is observed in grain boundaries of LSMO homostructure, to further exploit its potential, we study the quasiparticle dynamics of the LSMO homostructure with the spatial resolved ultrafast pump-probe microscopy.

Study of the ablation thresholds of monolayer MoS₂ from femtosecond to picosecond regime

Yin-Huan Gao¹, Li-Yang Jiang¹, Yu-Chan Tai¹, Chih-Wei Luo^{1,2,3,4,5}

¹Department of Electrophysics, National Yang Ming Chiao Tung University, Hsinchu 300, Taiwan.

²Institute of Physics and Center for Emergent Functional Matter Science, National Yang Ming Chiao Tung University, Hsinchu 300, Taiwan.

³National Synchrotron Radiation Research Center, Hsinchu 300, Taiwan.

⁴Taiwan Consortium of Emergent Crystalline Materials (TCECM), National Science and Technology Council, Taiwan.

⁵Department of Physics, University of Washington, Seattle, Washington 98195, USA.

liyangjiang.sc11@nycu.edu.tw; cwluoep@nycu.edu.tw

Abstract: We utilized a single-shot pulsed laser to ablate monolayer MoS₂, employing both Ti:sapphire and Yb-KWG lasers. Ablation areas were measured under varying dispersion conditions. The Ti:sapphire laser covered a pulsewidth range from 60 fs to 2 ps, while the Yb-KWG laser, with multiplate compression (MPC), covered a range from 4.9 fs to 97 fs. Through the relationship between ablation area and pulse energy, we calculated spot sizes and ablation thresholds under different dispersion conditions. Our observations show a decrease in the ablation threshold as pulsewidth decreases. This ablation thresholds-pulse dispersion relation was categorized into three intervals; ionization mechanisms, coulomb interaction in the many-body effect, and bandgap renormalization effects can explain each trend

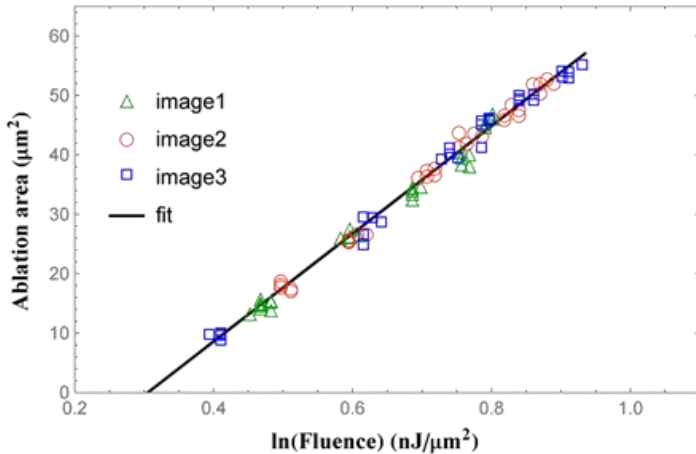


Figure 1: Ablation area versus natural logarithm energy density relationship diagram

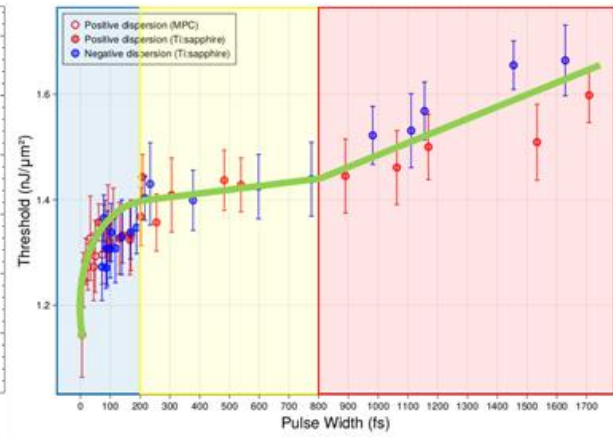


Figure 2: Variation of ablation threshold under different pulsewidths

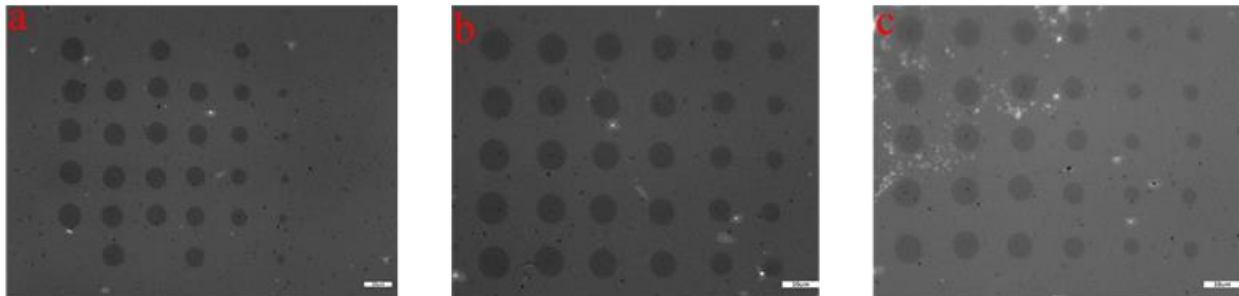


Figure 3: OM images of pulse ablation (a) image1 (b) image2 (c) image3

References

- [1] J. M. Liu, "Simple technique for measurements of pulsed Gaussian-beam spot sizes", *Optics Letters* 7(5), 196-198, (1982).

Ultrafast Electron Dynamics in 1T-TiSe₂ by Tr-ARPES

Shih-Chi Hung^{1,2}, Zhi-Ling Chen^{1,2}, Sheng-Chiao Wang^{1,2}, Hao-Hsiang Jia^{2,3}, Woei-Wu Pai⁴
Chih-Wei Luo¹, Ping-Hui Lin²

¹Department of Electrophysics, National Yang Ming Chiao Tung University, Hsinchu, Taiwan

²National Synchrotron Radiation Research Center, Hsinchu, Taiwan

³Institute of Photonics Technologies, National Tsing Hua University, Hsinchu, Taiwan

⁴Center for Condensed Matter Sciences, National Taiwan University, Taipei, Taiwan
shih.sc11@nycu.edu.tw

Abstract: Investigating the underlying mechanism of the charge density wave (CDW) phenomenon is crucial in condensed matter physics. We study the ultrafast electron dynamics in 1T-TiSe₂ within femtosecond scale via time- and angle-resolved photoelectron spectroscopy (Tr-ARPES). By extracting the transient evolution of the electron population, we provide a dynamic figure to describe the electron-hole pair generation and the electron-phonon interaction within TiSe₂.

1. Introduction

Charge density waves (CDWs) are an important part of the phase diagrams of many related electronic systems[1]. CDW materials undergo phase transitions at low temperatures, resulting in new electron density translational periodicity and periodic lattice distortion (PLD). In TMD 1T-TiSe₂, the phase transition occurs below T_c=200 K [2]. Therefore, the understanding of the CDW transition mechanism of this material has attracted considerable interest, especially for its driving mechanism. Meanwhile, some theoretical models have exhibited that the stability of CDW can be mutually reinforced through the combined effects of interband Coulomb interactions and electron-phonon coupling. Investigating the underlying mechanism of the CDW phenomenon is crucial in condensed matter physics. We performed time- and angle-resolved photoelectron spectroscopy (Tr-ARPES) measurements to resolve the ultrafast electron dynamics in 1T-TiSe₂ in CDW and normal phase. Through comparing the transient electron population within particular energy and momentum, we are able to track the temporal evolution and scattering pathway of the photoexcited electrons in both CDW and normal phases.

2. Figures

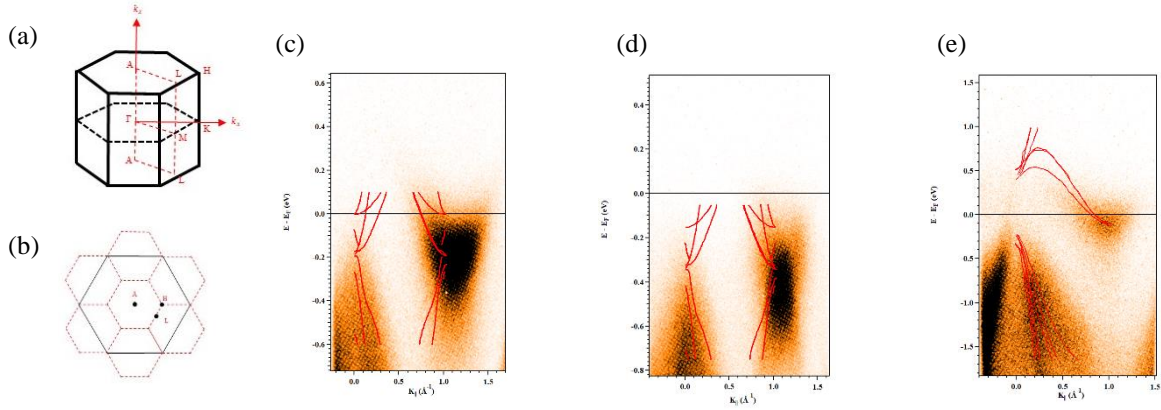


Figure 1. Crystal structure and electronic band structure of TiSe₂ measured by Tr-ARPES (a) Brillouin zones of TiSe₂ (b) Representation of two-dimensional at the $k_2 \sim \pi$ plane. (c-e) Band dispersions along high symmetry A-L direction, probed with 42 eV at timezero after 800 nm excitation. The spectra were obtained with temperatures and fluences of (c) 78 K and F = 0.70 mJ/cm², (d) 78 K and F = 0.09 mJ/cm², (e) 300 K and F = 2.23 mJ/cm², respectively. The red solid lines obtained from Ref. [3][4] for the calculated band structure in CDW and non-CDW phases.

3. Equations

$$I(t) = A_0 \exp\left(-\frac{t}{\tau_0}\right) + A_1 \exp\left(-\frac{t}{\tau_1}\right)$$

4. References

- [1] H.Hedayat, *Excitonic and lattice contributions to the charge density wave in 1T-TiSe₂ revealed by a phonon bottleneck* (Phys. Rev. R,2019), 1,023029.
- [2] Monney C, Puppini M. *Revealing the role of electrons and phonons in the ultrafast recovery of charge density wave correlations in 1T-TiSe₂*. (Phys. Rev. B.,2016), 94,165165.
- [3] T. Jaouen, *Phase separation in the vicinity of Fermi surface hot spots* (Phys. Rev. B,2019), 100, 075152.
- [4] Maria Hellgren, *Critical Role of the Exchange Interaction for the Electronic Structure and Charge-Density-Wave Formation in TiSe₂* (Phys. Rev. L,2017), 119, 176401.

Terahertz Emission Spectroscopy of Topological Material EuCd_2As_2 Single Crystals

Yi-Cheng Cheng¹, Po-Wei Gong¹, Pei-Tsung Yang¹, Xin-Yun Chang¹, Jiun-Haw Chu²,
Cheng-Chien Chen³, Jiunn-Yuan Lin⁴, Chih-Wei Luo¹, and Chien-Ming Tu¹

¹Department of Electrophysics, National Yang Ming Chiao Tung University, Hsinchu, 300093 Taiwan

²Department of Physics, University of Washington, Seattle, WA, 98195 USA

³Department of Physics, University of Alabama at Birmingham, Birmingham, AL, 35294 USA

⁴Institute of Physics, National Yang Ming Chiao Tung University, Hsinchu, 300093 Taiwan

Author e-mail address: (8-point type, centered, italicized)

Abstract: We use the terahertz emission spectroscopy to study the ultrafast carrier dynamics of EuCd_2As_2 single crystal, by changing the helicity of incident optical pulses. By time domain decomposition and recombination, circular photogalvanic effect (CPGE) signal originated from spin-polarized currents were obtained. The CPGE signal strongly depend on the incident angle of incident optical pulses, and almost no CPGE signal was observed at normal incident case. These observations agree with the features of a two-dimensional electron system. Rashba effect would be a potential candidate for these observations on EuCd_2As_2 single crystals at room temperature.

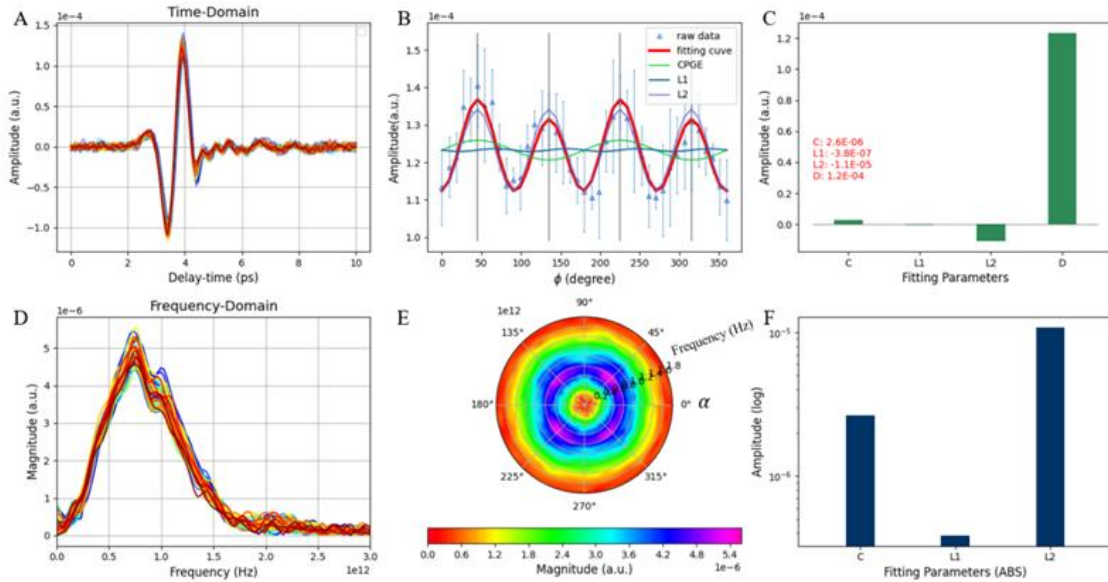


Figure 1. Use quarter wave plate alpha-scan with 45 degree incidence analysis. (A) time-domain terahertz signals under different helicities, (B) extracting positive peaks for model fitting, (C) comparison of fitting parameters, (D) Fourier transform into terahertz spectrum under different helicities, (E) 2D contour plot of frequency-domain spectrum versus angle, (F) Ratio of absolute values of fitting parameters.

$$E_{THz}(\alpha, t) \propto \frac{\partial j(t)}{\partial t} = C'(\alpha, t) \sin(2\alpha) + L_1'(\alpha, t) \sin(4\alpha) + L_2'(\alpha, t) \cos(4\alpha) + D'(\alpha, t) \quad (1)$$

References

- [1] N. P. Armitage, et al., "Weyl and Dirac semimetals in three-dimensional solids", Rev. Mod. Phys. 90. 015001 (2018)
- [2] Yuto Kinoshita, et al., "Terahertz radiation by subpicosecond spin-polarized photocurrent originating from Dirac electrons in a Rashba-type polar semiconductor", Phys. Rev. B 97. 161104 (2018)
- [3] J.-Z. Ma, S. M. Nie, C. J. Yi, et al., "Spin fluctuation induced Weyl semimetal state in the paramagnetic phase of EuCd_2As_2 ", Science advances, vol. 5, no. 7, eaaw4718 (2019)

Photoinduced evolution of effective mass in 1T-TiSe₂

Zhi-Ling Chen^{1,2}, Shih-Chi Hung^{1,2}, Sheng-Chiao Wang^{1,2}, Hao-Hsiang Jia^{2,3}, Woei-Wu Pai⁴,
Chih-Wei Luo^{1,*}, Ping-Hui Lin^{2,*}

¹Department of Electrophysics, National Yang Ming Chiao Tung University, Hsinchu, Taiwan

²National Synchrotron Radiation Research Center, Hsinchu, Taiwan

³Institute of Photonics Technologies, National Tsing Hua University, Hsinchu, Taiwan

⁴Center for Condensed Matter Sciences, National Taiwan University, Taipei, Taiwan

lynn.sc11@nycu.edu.tw

Abstract: We performed the ultrafast electron dynamics of the charge density wave (CDW) material 1T-TiSe₂ using the time- and angle-resolved photoemission spectroscopy (TR-ARPES) system. The experimental results provide a direct visualization of the Ti-3d conduction band and the corresponding evolution of effective mass as a function of pump fluence. The data show that the effective mass of the Ti-3d electron pocket become heavier as pump fluence increase, which indicates the degree of CDW phase destroyed at different photoexcitation densities. We also present the time evolution of Ti-3d band and the change of effective mass suggest the recovery of the CDW phase.

1. Introduction

1T-TiSe₂ is a transition metal dichalcogenide (TMD) material. Previous ARPES reports has elucidated that its electronic structure is primarily composed of the Se-4p valence band located at the A point and the Ti-3d conduction band at the L point of the Brillouin zone, respectively. Notably, below $T_c \cong 200$ K, TiSe₂ undergoes a charge density wave (CDW) phase transition characterized by a $2 \times 2 \times 2$ ordering. Such transition leads to a backfolding of the Se 4p band to the L point[1,2].

In this study, we delve into the dispersion of the Ti-3d band at the L point above E_F using TR-ARPES. Our observations reveal the band renormalization and an increase in effective mass after excitation. By correlating the effective mass with pump fluence, we found that the CDW phase can be completely destroyed beyond a certain fluence threshold. As the fluence increase, the effective mass becomes heavier, indicating the greater disturbance and longer recovery time of CDW phase. Such transient melting of CDW order was previous reported in optical pump-probe measurements on rare-earth tritellurides material LaTe₃, where the oscillation of the CDW order persists only at low fluence without complete breakdown[3]. Consequently, we declare that analyzing the evolution of the effective mass of the Ti-3d electron pocket as a function of pump fluence provides deeper insights into the intricate interactions in 1T-TiSe₂.

2. Figures

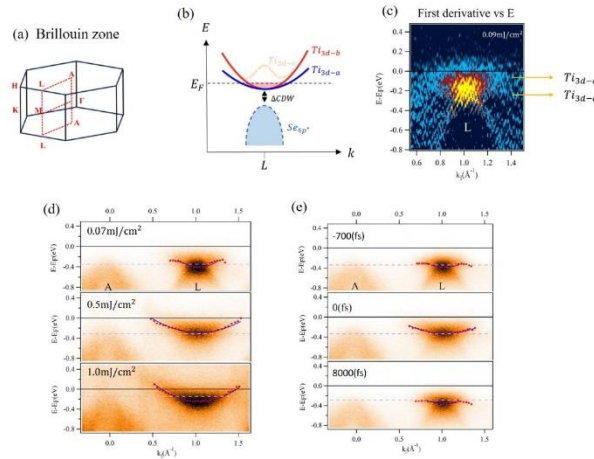


Figure 1. (a) Brillouin zone of 1T-TiSe₂ with high symmetry labels. (b) Schematic diagram of the band structure in CDW phase. (c) Second-derivative band dispersion at L-point after excitation with fluence of 0.09 mJ/cm^2 . (d) The fluence-dependent spectra along A-L direction at timezero measured with $F = 0.07 \text{ mJ/cm}^2$ to 1.0 mJ/cm^2 . The solid lines indicates the fitting curves. (e) TR-ARPES spectra along A-L direction in equilibrium and after excitation with 800 nm pump pulses at 0.2 mJ/cm^2 fluence.

3. Equations

$$\frac{1}{\hbar^2} \frac{d^2 E}{dk^2} = \frac{2a}{\hbar^2} = \frac{1}{m^*}$$

4. References

- [1] Huber, M. et al. "Mapping the dispersion of the occupied and unoccupied band structure in photoexcited 1T-TiSe₂". *Journal of Physics and Chemistry of Solids* 168, 110740 (2022).¹
- [2] C.Monney et al, "Dramatic effective mass reduction driven by strong electronic correlations". *Europhysics Letters* ,92(2010) 47003.
- [3] Dolgirev, P. E. et al. " Amplitude dynamics of the charge density wave in LaTe₃ : Theoretical description of pump-probe experiments. ". *Physical Review B* 101 (2020).

Ultrafast dynamics of SrCd₂Sb₂ and SrCd₂As₂ single crystals using optical pump-probe spectroscopy

Nidhi Puri^{1†}, Jiunn-Yuan Lin¹, Chih-Wei Luo^{2,3,4,5,6}, Chien-Ming Tu², Wen-Yen Tzeng², Chi-Chen Tsai¹, Jiun-Haw Chu³, Cheng-Chien Chen⁷

¹Institute of Physics, National Yang Ming Chiao Tung University, Hsinchu 30010, Taiwan

²Department of Electrophysics, National Yang Ming Chiao Tung University, Hsinchu 30010, Taiwan

³Department of Physics, University of Washington, Seattle, Washington 98195, USA

⁴Taiwan Consortium of Emergent Crystalline Materials (TCECM), National Science and Technology Council, Taiwan.

⁵Institute of Physics and Center for Emergent Functional Matter Science, National Yang Ming Chiao Tung University, Hsinchu, 30010, Taiwan

⁶National Synchrotron Radiation Research Center, Hsinchu, 30076, Taiwan.

⁷University of Alabama at Birmingham, Birmingham, Alabama, US

Author e-mail address[†]: nidhi.puri@nycu.edu.tw

Abstract: Topological insulators (TIs) represent a novel category of quantum materials characterized by their insulating properties in the bulk, accompanied by robust gapless surface states known as topological surface states (TSS). These surface states exhibit a unique behavior wherein the spin direction of electrons is locked perpendicular to their momentum due to the strong influence of spin-orbit interaction [1,2]. TIs have gained significant attention for their potential to uncover fascinating physics and to pave the way for various applications in fields like optoelectronics, spintronics, and quantum computing [1-4]. In this context, the present study utilizes AB₂X₂ type SrCd₂Sb₂ single crystals to study the ultrafast dynamics of carriers and phonons to gain insight into critical changes in crystal structure. Here, a powerful technique of optical pump-probe (OP-OP) spectroscopy (Fig. 1a) in studying dynamic electronic processes, was employed to investigate the response of as-synthesized SrCd₂Sb₂ and SrCd₂As₂ single crystals under ultrafast laser excitation. To obtain the best-fit to $\Delta R/R$ curve, a tri-exponential function has been used and the parameters have been tabulated in the Fig. 1 below. The significant observations from the OP-OP measurements include, (i) absence of sub-ps τ_1 decay component in SrCd₂Sb₂, (ii) appearance of ~ 10 ps decay term (τ_3) for SrCd₂Sb₂, and (iii) the change of sign for the amplitude (A_2) of several ps τ_2 decay term. The results revealed contrast ultrafast dynamics between SrCd₂As₂ and SrCd₂Sb₂ thereby implying that SrCd₂As₂ and SrCd₂Sb₂ have distinct electronic structures near the band edge. The transient reflectivity ($\Delta R/R$) curve (Fig. 1b) shows a sharp rise followed by a slow decay. A detailed analysis on the current results will provide deeper understanding on the underlying physics of the electronic structure of SrCd₂Sb₂ single crystals.

We are grateful to NSTC of Taiwan and AFOSR of US for supporting this project (NSTC-110-2124-M-A49-007-MY3).

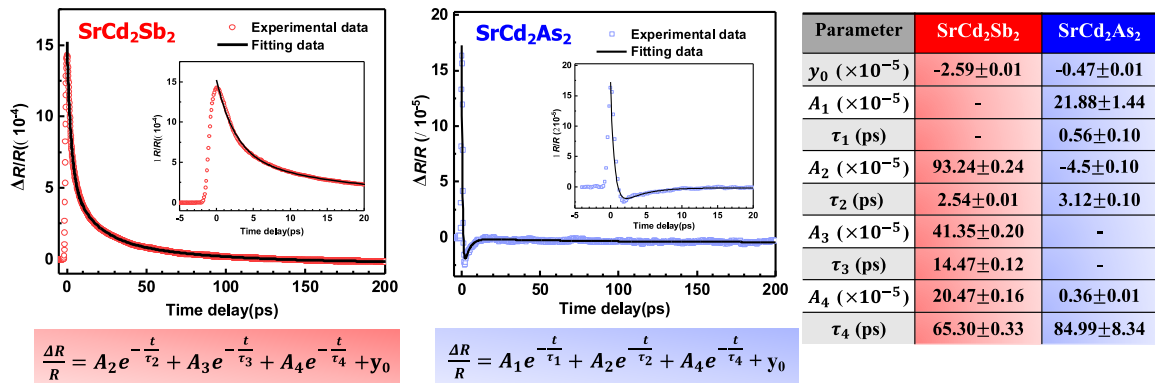


Fig. 1. The transient reflectivity ($\Delta R/R$) curves obtained from the OP-OP spectroscopy. The table on the right side shows the fitting parameters estimated from the tri-exponential fitting function.

References

- [1] J.E. Moore, "The birth of topological insulators", Nature, 194-198, 464 (2010).
- [2] M.Z. Hasan, C.L. Kane, "Topological insulators", Rev. Mod. Phys. 3045-3067, 82 (2010).
- [3] C.W. Luo et al, "Snapshots of dirac fermions near the dirac point in topological insulators", Nano Lett., 5797-5802, 13 (2013).
- [4] C.-M. Tu et al., "Manifestation of a second Dirac surface state and bulk bands in THz radiation from topological insulators", Sci. Rep., 14128, 5 (2015).

Temperature dependent ultrafast dynamics of topological material EuCd_2Sb_2

Chi-Chen Tsai^{1†}, Jiunn-Yuan Lin¹, Jiun-Haw Chu³, Cheng-Chien Chen⁷, Nidhi Puri¹, Yu-Sheng Kuo¹,
Wen-Yen Tzeng², Chien-Ming Tu², Chih-Wei Luo^{2,3,4,5,6}

¹Institute of Physics, National Yang Ming Chiao Tung University, Hsinchu 30010, Taiwan

²Department of Electrophysics, National Yang Ming Chiao Tung University, Hsinchu 30010, Taiwan

³Department of Physics, University of Washington, Seattle, Washington 98195, USA

⁴Taiwan Consortium of Emergent Crystalline Materials (TCECM), National Science and Technology Council, Taiwan.

⁵Institute of Physics and Center for Emergent Functional Matter Science, National Yang Ming Chiao Tung University, Hsinchu, 30010, Taiwan.

⁶National Synchrotron Radiation Research Center, Hsinchu, 30076, Taiwan.

⁷University of Alabama at Birmingham, Birmingham, Alabama, US

Author e-mail address[†]: godtsai310195@gmail.com

Abstract: Topological materials (TMs) have recently gained attention due to their potential physical properties for applications in spintronics devices and quantum computing [1-4]. Topological insulators (TIs), one kind of TMs, exhibit conducting surface states protected by time-reversal symmetry, and the gapless surface states are resulted from band inversion as well as spin-orbit coupling. In this study, we report on the ultrafast carrier dynamics of TM EuCd_2Sb_2 single crystals by two-color optical pump-optical probe (OP-OP) technique (Fig. 1a). A long-cavity Ti:sapphire oscillator (XL300, FemtoLaser Inc.) was employed to generate 400-nm optical pulses for pump and 800-nm optical pulses for probe beam. The time-domain traces of transient reflectivity ($\Delta R/R$) of the probe pulses were recorded in the temperature range of 2-300 K. The $\Delta R/R$ curve for 300 K and 2 K (Fig. 1b) shows negative and positive signal, respectively. In addition, we also applied a magnetic field of 6 T horizontal to the c-axis of the sample and performed the OP-OP measurements in the temperature range of 2-30 K. The detailed analysis of these results will be carried out to have a deeper understanding on the ultrafast dynamics of EuCd_2Sb_2 single crystals.

We are grateful to NSTC of Taiwan and AFOSR of US for supporting this project (NSTC-110-2124-M-A49-007-MY3).

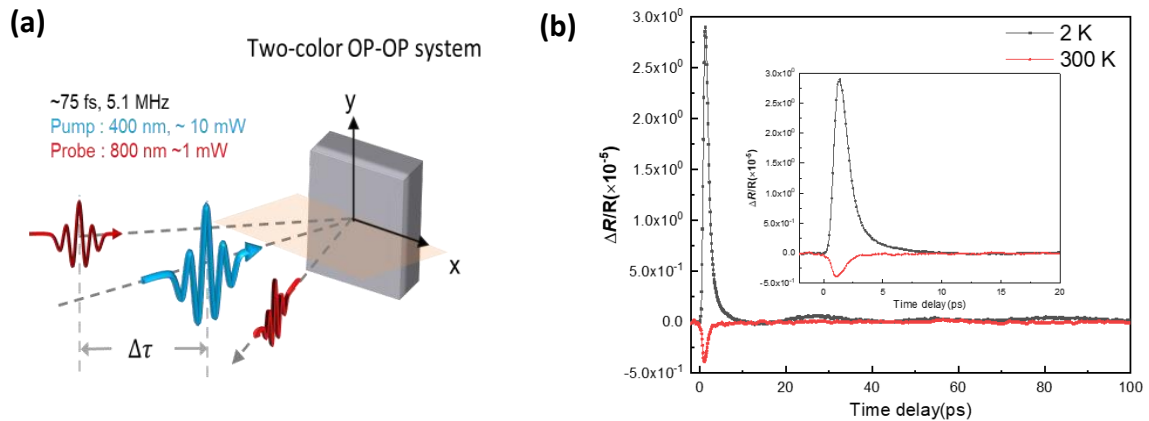


Fig. 1.(a) Schematic diagram for OP-OP system (b) The transient reflectivity curve for EuCd_2Sb_2 result at room temperature and 2 K in time domain.

References

- [1] J-M. DeStefano, L-L Wang, Phys. Rev. B 103, 115207 (2021).
- [2] J.E. Moore, "The birth of topological insulators", Nature, 194-198, 464 (2010).
- [3] M.Z. Hasan, C.L. Kane, "Topological insulators", Rev. Mod. Phys. 3045-3067, 82 (2010).
- [4] M. Z. Hasan and J. E. Moore, "Three-Dimensional Topological Insulators", Ann. Rev. Condensed Matter Physics 2, 55-78 (2011).

Ultrafast carrier dynamics of SWCNT under existence of amino acids

Chia-Hung Lin , Atsushi Yabushita , Chih-Shian Wang

Department of Electrophysics, National Yang Ming Chiao Tung University, Science Building III, No 1001, University Rd., Hsinchu 300, Taiwan

Author e-mail address: lsp94161@gmail.com

Abstract: In this work, the home-made NOPA (Non-collinear optical parametric amplifier) system is used to study the carrier dynamics of single-walled carbon nanotubes and amino acid solutions. Through the NOPA system, the visible probe light of about 10 femtosecond pulses and the multichannel lock-in amplifier are used to analyze the ultrafast transient absorption spectrum detected in the visible light band (500nm~700nm). Carrier dynamics of carbon nanotubes mixed with amino acids.

Global fitting analysis estimates the two times of in-band relaxation and inter-band relaxation to be 50fs~100fs and 500fs~1ps, respectively. The analysis results show that addition of amino acids change the relaxation time of the carriers in the SWCNTs reflecting initial interaction mechanism between SWCNTs and amino acids.

1. Introduction

In the non-covalent modification method, dispersants such as surfactants, polymers, proteins, etc., have been widely studied in the aqueous dispersion of carbon nanotubes. However, these studies mainly focus on a few dispersants, and a deeper understanding of the dispersing properties and stabilizing effects of other amino acids is still lacking. In addition, amino acids are an elementary unit for composing proteins and determine their chemical properties, thus, this work shed light on the interactions between CNTs and proteins in femtosecond region, to understand the biological effects CNTs of and lead to potential biological applications.

2. Materials and methods

The laser system used in this experiment is the NOPA, after adjusting the pulse compression, by the second-harmonic generation frequency-resolved optical gating can finally compress the pulse width to less than 10fs[1,2]. The schematic diagram of the system is shown in Figure 1.

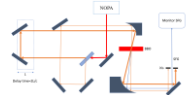


Fig. 1. NOPA system

3. Experimental results

Using global fitting analysis, the Figure 2-5 shows the Transient absorption (TA) rate changes of the four sample in the long-time range of 672nm. The black line is the absorptivity change of the actual measurement, and the red line is the fitting result:

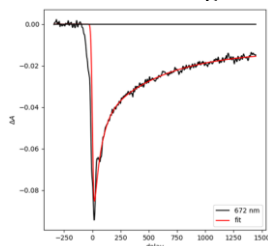


Fig.2 . SWCNT

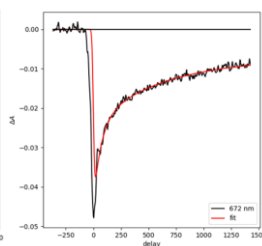


Fig.3 . SWCNT + Arginine

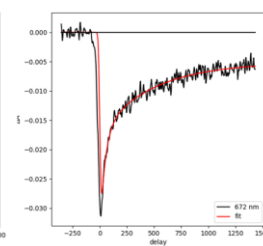


Fig.4 . SWCNT + Histidine

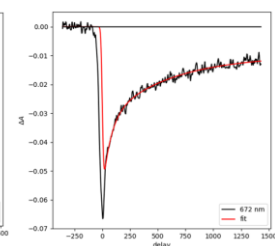


Fig.5 . SWCNT + Lysine

4. Conclusion

In this experiment, two kinds of relaxation times are estimated to be about 50fs~100fs and 500fs~1ps, representing the intra-band relaxation time and inter-band relaxation time respectively.

5. Reference

- [1] T. Kobayashi, A. Baltuska, Meas. Sci. Technol. 13, 1671-1682 (2002).
- [2] C. J. Bardeen, Q. Wang, C. V. Shank, Phys.Rev. Lett. 75, 3410 (1995).

Ultrafast dynamics of carbon nanotubes with different chiralities

Hsuan Yu Ou, Sai Shuwen, Atsushi Yabushita

Department of Electrophysics, National Yang Ming Chiao Tung University, Hsinchu 300, Taiwan, ROC
E-mail: hsuanyu.sc11@nycu.edu.tw

Abstract: Ultrafast spectroscopy was employed to investigate purified and unpurified single-walled carbon nanotubes (SWCNTs), revealing three relaxation processes with rates of 10, 2, and 0.5 ps⁻¹, respectively. The fastest one originated from intraband relaxation in the electronic excited state, while the other two involved interband relaxation, returning electrons to the ground state. The unpurified sample exhibited molecular intermolecular vibrational energy transfer.

1. Introduction

Single-wall carbon nanotubes (SWCNTs) [1] have garnered significant attention due to their properties lying between those of fullerene and graphene. Their high tensile strength makes them suitable for applications like armor and composite materials, while their exceptional thermal conductivity offers advantages in fields such as space elevators. The electrical conductivity of SWCNTs is influenced by their chirality (n, m), and spectroscopic techniques can characterize this chirality. Time-resolved studies employing femtosecond pulses of 10 fs investigate photoexcitation, exciton formation, and dynamics. Ultrafast absorption spectroscopy unveils electronic and RBM dynamics in SWCNTs of varying chiralities. This research deepens our comprehension of SWCNT properties and optical behavior, holding significant implications for future applications and advancements in biosensing [2].

2. SWCNT samples

Commercially available (6,5) single-walled carbon nanotubes (SWCNTs) containing other chiralities were used, and no further purification was conducted. In the experiment, SWCNTs were dispersed in water containing sodium dodecyl sulfate (SDS) using ultrasonication, followed by centrifugation in a high-speed centrifuge. Sodium dodecyl sulfonate (SDS) was used for separation, and SWCNTs were subjected to chirality sorting using the JASCO chromNAV system. Ultimately, purified (6,5) SWCNT samples were obtained and subjected to optical measurements in water containing sodium cholate (SC).

3. Results and discussion

We conducted spectral measurements on two types of nanotube samples, non-purified and purified, with a focus on the spectral region of 612–630 nm (see Fig. 1). In the 612–630 nm range, the RBM of the non-purified sample exhibited an upward trend (see Figure 1a). This change could arise from two mechanisms. The first possibility is the overlap of RBMs with different frequencies. However, the observed traces are unlikely to reflect such overlap. The second possibility is energy transfer between different chiralities, but considering the diameter differences of the samples, a single nanotube cannot contain both chiralities simultaneously. Therefore, we attribute the observed upward shift to energy transfer between nanotubes of different chiralities. In the non-purified sample, the RBM frequency appears to approach that of the (6,4) chirality, while it remains stable in the purified sample. Simultaneously, for the non-purified sample, the transient absorption signal in the 612–630 nm region exhibited positive (negative) values, reflecting induced absorption from the electronically excited state (ground-state bleaching) (see Fig. 2).

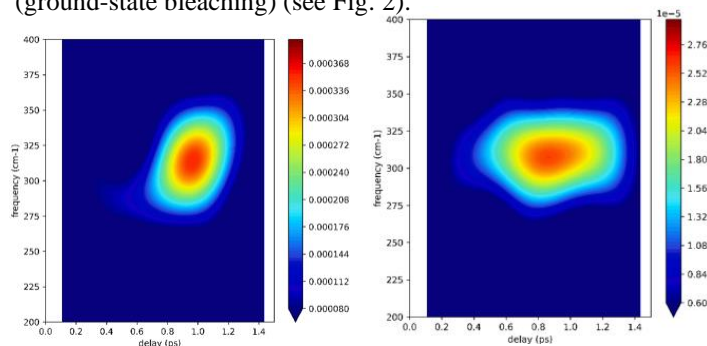


Fig. 1. Spectrogram traces of the (a) non-purified (b) purified

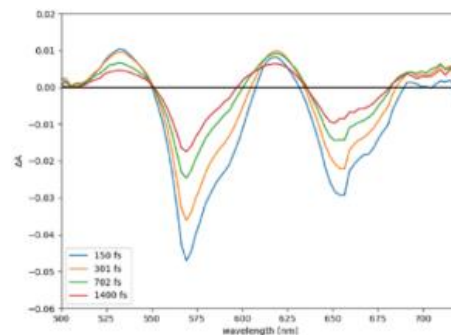


Fig. 2. Transient absorption spectra $\Delta A(\lambda, t)$ for non-purified

4. References

- [1] S. Iijima, T. Ichihashi, Single-shell carbon nanotubes of 1-nm diameter, *Nature* 363 (1993) 603–605.
- [2] C.M. Tilmaciu, M.C. Morris, Carbon nanotube biosensors, *Front. Chem.* 3 (2015) 59

Ultrafast dynamics of CongoRed under adsorption

ChiaYun Cheng, WeiXiang Huang, Atsushi Yabushita
National Yang Ming Chiao Tung University Department of Electronphysics
ellen8973@gmail.com

Abstract: Using Ultraviolet pump and white light probe (UPWP) system, a harmonic pulse centered at 400nm wavelength is used to make the sample go from the ground state to the excited state, and use broadband WLC pulse detection light to analyze the ultrafast kinetics of the Congo red sample. The clear and complete record of the ultrafast dynamic response detected in the wave band (500~750 nm) is used to calculate the decay spectrum (DAS) and its lifetime. We observed that at higher laser power, the decay time is shorter.

1. Material and methods

Congo red (CR) studied in this work, is known to bind to amyloid proteins and thought to be useful for characterization of amyloid formation in Alzheimer patients [1]. Using the system described below, we have performed ultrafast spectroscopy for an aqueous solution of CR (CR-H₂O) and a water dispersed solution of CR adsorbed on a particle of hydroxyl apatite (CR-HA).

Using Ultraviolet pump and white light probe (UPWP) as Fig. 1. The light source emits near-infrared (NIR) pulses, which are then split into two pulses by a beam splitter. The higher intensity NIR pulse is focused on β -BaB₂O₄ (BBO crystal) to generate a 400 nm second harmonic (SH) pulse, which is used to excite the sample from the ground state to the excited state. The lower intensity NIR pulse is focused on a 2mm thick sapphire plate, producing a wideband white-light continuum pulse (WLC) due to focusing effects and third-order susceptibility. A short-pass filter is used to eliminate spectral components above 750nm, and this WLC pulse is used as the probing pulse. After passing through the sample, the light is dispersed through an optical fiber and coupled into a photodiode array (PDA) camera. The excitation pulses are modulated at a frequency of 2.5 kHz using an optical chopper. The spectrum obtained from the PDA camera observes the difference in absorption between the presence and absence of the excited sample.

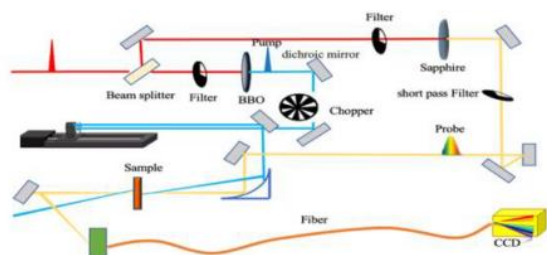


Fig. 1. UPWP system

2. Results and discussion

We conducted ten cycles of scans to obtain the average measurement, generating a substantial amount of data of variation in transmittance ΔT . By analyzing this data, we obtained transient absorption ΔA , which was then subjected to global fitting to determine the decay time then calculate the average decay time τ for each laser power. Comparing the results between CR-HA and CR-H₂O samples, we observed that at higher laser power, the decay time was shorter. This could be attributed to the higher power laser providing more energy, accelerating the interaction between light and matter, resulting in faster generation of photoproducts. Furthermore, due to the closer proximity of CR-HA molecules adsorbed on Hydroxyapatite, there might be an enhancement of accelerated photopolymerization and photoproduct generation [2,3]. In contrast in the CR-H₂O sample, where the molecules are more spaced apart, the generation of photoproducts is slower. Overall, we noted a negative correlation between laser power and decay time.

3. References

- [1] Styren, S. D.; Hamilton, R. L.; Styren, G. C.; Klunk, W. E., (2000), A fluorescent derivative of Congo red: A novel histochemical stain for alzheimer's disease pathology. *J. Histochem. Cytochem.* 48(9), 1223–1232.
- [2] Heyne, B. (2016). Self-assembly of organic dyes in supramolecular aggregates. *Photochemical & Photobiological Sciences*, 15, 1103-1114.
- [2] Chen, Z., Lohr, A., Saha-Möller, C. R., & Würthner, F. (2009). Self-assembled π -stacks of functional dyes in solution: structural and thermodynamic features. *Chemical Society Reviews*, 38(2), 564-584.